Evaluation of Intelligent Surfaces in Railroad Communication

Master's Thesis 2021

for obtaining the academic degree

Dipl.-Ing.

as part of the study

Telecommunications

carried out by

Kevin Niederwanger

student number: 01525861

Institute of Telecommunications

at TU Wien
AT-1040 Vienna
Gußhausstraße 25/E389
Telephone (+43 1) 58801

Main-advisor: Asst. Prof. Dipl.-Ing. Dr.techn. Stefan Schwarz
Co-advisor: Projektass. B.Sc. Dipl.-Ing. Bashar Tahir

Code of Conduct

Hiermit erkläre ich, dass die vorliegende Arbeit gemäß dem Code of Conduct – Regeln zur Sicherung guter wissenschaftlicher Praxis (in der aktuellen Fassung des jeweiligen Mitteilungsblattes der TU Wien), insbesondere ohne unzulässige Hilfe Dritter und ohne Benutzung anderer als der angegebenen Hilfsmittel, angefertigt wurde. Die aus anderen Quellen direkt oder indirekt übernommenen Daten und Konzepte sind unter Angabe der Quelle gekennzeichnet. Die Arbeit wurde bisher weder im In– noch im Ausland in gleicher oder in ähnlicher Form in anderen Prüfungsverfahren vorgelegt.

Vienna, August 2021

Kevin Niederwanger

Acknowledgements

I would like to express my gratitude to my supervisors Asst. Prof. Dipl.-Ing. Dr.techn. Stefan Schwarz and Projektass. B.Sc. Dipl.-Ing. Bashar Tahir for the useful comments, remarks and engagement through the learning process of this thesis. Furthermore, I would like to thank my advisors for introducing me to the topic as well for the support on the way. I would like to thank my loved ones, who have supported me throughout the entire process, both by keeping me harmonious and helping me assemble the pieces.
I would also like to thank Univ.Prof. Dipl.-Ing. Dr.techn. Markus Rupp for giving me the opportunity to work on the Vienna Cellular Communications Simulators (VCCS) which gave me an advanced insight into the topic of wireless communications and enhanced my interest.
The valuable practical information from Dipl.-Ing. Dr. Martin Taranetz and Ing. Richard Hintersteiner was greatly appreciated.
The financial support by the Austrian Federal Ministry for Digital and Economic Affairs, the Austrian National Foundation for Research, Technology and Development, and the Christian Doppler Research Association is gratefully acknowledged.

Abstract

Public transport is gaining more and more popularity throughout the world. As a consequence, the amount of users connected to the mobile network while traveling in trains keeps rising. Each user has different needs considering data rates, latency and reliability while traveling eco-friendly for several thousand kilometers per year in many places across the world. Providing the best possible quality of service to the aforementioned properties is the future of wireless networks beyond 5th generation (5G). Enabling all of these features is a challenging task, especially for railroad communications. This field of wireless communications has to deal with large distances, high velocity and many users, simultaneously. A potential candidate for the upcoming 6th generation (6G) network devices are Reconfigurable Intelligent Surfaces (RISs). A RIS consists of an array with electromagnetically reconfigurable elements in order to modify the response to incident signals.

In this thesis, several use cases for intelligent surfaces in a railroad environment are discussed. A very promising case of application is to use a RIS to overcome Non-Line-Of-Sight (NLOS) situations. At first, this scenario is evaluated in terms of link level simulations. A power scaling law, impact of the K-factor of the employed Rician channel model and different imperfections are taken into consideration. After studying this topic, system level simulations are used to evaluate the impact of a RIS, if it has to cover an entire area. The scenario is rebuilt with realistic geometrical information from a railroad scenario in Austria. A major contribution is the analysis of different placement strategies for a RIS as well as the impact of two beamforming schemes. At the end of the thesis, a concluding example with a noticeable performance gain through a RIS is presented.

Kurzfassung

Der Bahnverkehr wird ein immer wichtigerer Teil unserer Gesellschaft. Durch diese steigende Popularität wächst auch die Anzahl der Fahrgäste. Jede(r) einzelne dieser Gäste ist mit dem Mobilfunknetzwerk verbunden und besitzt unterschiedliche Anforderungen an Datenraten, Latenzzeiten und Zuverlässigkeit. Die bestmögliche Kundenzufriedenheit zu erreichen ist unter anderem eines der Hauptthemen des künftigen 6G Mobilfunks. Speziell für den Bahnverkehr ist es schwierig diese Anforderungen zu erfüllen, weil durch die großen Distanzen, hohen Geschwindigkeiten und gleichzeitig vielen Benutzern ein sehr forderndes Umfeld geschaffen wird. Rekonfigurierbare intelligente Oberflächen sind ein möglicher Kandidat um all diesen Anforderungen gerecht zu werden. Hierbei handelt es sich um Materialien/Oberflächen, deren elektromagnetische Reflexions/Absorptions-Eigenschaften mittels einer Zellstruktur elektronisch modifiziert werden können. Dadurch ist es z.B. möglich am Ort des Empfängers ein erhöhtes Signal-Rausch-Verhältnis zu erzielen.
Diese Diplomarbeit beschäftigt sich mit möglichen Anwendungsfällen von rekonfigurierbaren, intelligenten Oberflächen für das Eisenbahnwesen. Ein sehr vielversprechendes Einsatzgebiet ist das Verwenden solch einer Oberfläche um eine indirekte Sichtverbindung herzustellen. Dieses Szenario wird ausgiebig in dieser Arbeit untersucht. Zuerst werden Bitfehlerraten mit Hilfe des verwendeten Rice Kanalmodells evaluiert. Darunter fällt die Auswirkung diverser Parameter, wie zum Beispiel des K-Faktors, als auch nicht optimale Eigenschaften intelligenter Oberflächen. Anschließend wird auch das Signal-Rausch-Verhältnis in einer realistischen Simulationsumgebung simuliert. Ein wichtiger Beitrag dieser Diplomarbeit befindet sich in der Analyse von unterschiedlichen Platzierungsstrategien um die Servicequalität zu verbessern und im Vergleich von zwei Methoden zur Anpassung der Antennen Abstrahlcharakteristik. Zum Abschluss wird eine Beispiellösung mit einer deutlichen Verbesserung durch eine intelligente Oberfläche präsentiert.

Contents

1 Introduction

1.1 Motivation

The research on beyond 5G technologies has already started. One important candidate technology for such systems is an Intelligent Reflective Surface (IRS) or equivalently Reconfigurable Intelligent Surface (RIS). This technology has recently gathered a lot of attention from industry and academia [1][2]. A RIS collects wireless signals from a transmitter and reflects them, ideally in an entirely passive manner, towards the receiver. During this reflection process, a controlled phase shift is introduced to the signal, such that every wavefront at the receiver interferes constructively, leading to a passive beamforming gain.
Intelligent surfaces are direct competitors with existing relay technology with the advantage of lower deployment costs and energy consumption due to their passive nature. This benefit makes this technology very promising for indoor, outdoor-to-indoor and even outdoor uses. A comparison between a RIS and a simple amplify-and-forward relay can be found in [3]. According to [3], the received power in case of a relay connection is inversely proportional to the fourth power of the distance between transmitter and receiver. Using an intelligent surface instead of a relay changes this behaviour under certain assumptions to a dependence on the second power of the distance. This drastic change in distance dependency makes using a RIS in a scenario with large distances, e.g. railroad, very appealing. Relaying is also a common method in railway scenarios to improve the quality of service, however, increasing frequencies in beyond 5G technologies leads to a higher demand on Line-Of-Sight (LOS) connections, which is a potential downside of using in-train repeaters. An intelligent surface could be placed in LOS to the transmitter and receiver simultaneously in order to provide an alternative solution to the common in-train repeaters. This forms the fundamental building block of this thesis, which is to investigate the performance of a RIS in a railroad scenario to overcome NLOS limitations.
Please note that using an intelligent surface in NLOS scenarios is not the only potential use case for railroad communications. Alternative approaches will be discussed based on available literature.

1.2 Objective and outline

The topic of this thesis is to analyze the performance impact of a RIS in a railroad scenario to overcome NLOS situations. In particular, this means that at some point the transmitter has no LOS to the receiver, but a reflective surface is placed such that it has LOS to both endpoints. The evaluation is done in terms of Bit Error Rate (BER) and Signal-To-Noise Ratio (SNR) simulations in Matlab [4], which provides a very detailed view of the system performance. This thesis provides answers to very crucial

questions, such as

- Is a performance gain with a RIS in a railroad scenario possible? In case it is, how can it be achieved?
- Are there alternative approaches that look promising?
- What is the impact of non-ideal reflective surfaces?
- Where should a RIS be placed in a railroad scenario? What are appropriate criteria for the placement?

In order to provide answers to all of these questions, this thesis is split up into three main chapters starting with a literature review. Chapter 2 provides an overview of the current research state for RISs. This is not entirely focused on railroad scenarios, especially because several benefits of reflective surfaces are neither limited nor analyzed in the context of railway scenarios. The discussion in this chapter provides amongst other things principle use cases, available measurement campaigns and different manufacturing strategies.
In Chapter 3 the basic behaviour of a RIS for link level simulations is discussed. This includes the channel modelling and the impact of the corresponding parameters. In addition, non-optimal surfaces, for example due to the manufacturing process, are considered.
Chapter 4 evaluates the performance impact of a RIS in terms of system level simulations. This means, that the RIS has to cover an entire area, which considers movement as static snapshot simulations. This chapter points out the importance of available measurement campaigns for railroad scenarios, in order to provide a realistic simulation environment. Different placement strategies for a RIS are discussed, alongside the possible performance gain and limitations.

2 State of the art

This chapter provides a literature review of RISs, highlighting current concepts, use cases and potential downsides. Detailed summaries about this topic can be found in [1] and [2]. Currently, there is no standardized solution available, and therefore multiple approaches can be considered viable.

2.1 Use cases in a railroad environment

This section discusses potential use cases for intelligent surfaces in a railroad environment. Only one of these approaches is discussed in the upcoming chapters, nevertheless all of them are surely worth further investigation.

2.1.1 Holographic beamforming

Holographic beamforming is the most generic approach for intelligent surfaces in railroad communication. This type of beamforming can be understood as using an active RIS which is connected to a Radio Frequency (RF) signal generator via cable to minimize losses. The name is given due to the similarity to the optical holography concept, which will be explained briefly. Two waves, i.e. a reference wave and an object wave, are superimposed at the surface in the training phase. The reference wave is generated by the RF signal generator, whereas the object wave is reflected from the desired user by, for example, a pilot signal. The superimposed field will be recorded at the so called Holographic Multiple Input Multiple Output Surface (HMIMOS) and can be reconstructed in the second, i.e. communication, phase. During the communication phase, the reconstructed electromagnetic wave interferes constructively at the desired user. The HMIMOS effectively operates as a beamformer similar to a phased array antenna, but it is constructed in a different way. These surfaces can be manufactured continuous or discrete by, for example, using varactor diodes. The bias voltage of the diodes controls the impedance and consequently the reflection phase, amplitude states and phase distribution [5]. Comparing an active phased array antenna with the holographic beamformer reveals that HMIMOS use a larger amount of elements while requiring only one RF chain, whereas phased array antennas usually have one amplifier at every radiating element. For this reason, holographic beamforming antennas are less power hungry and more efficient than active phased array antennas. A comparison of these two technologies can be found on the leading company's (Pivotal Commware) website where a similar antenna gain can be achieved while simultaneously the HMIMOS consumes only one-third of the power of the active phased array antenna [6].

2.1.2 Reflector

Using a RIS as a reflective device similar to a mirror, albeit not equivalent, is the case of application which will be discussed in Chapter 3 and Chapter 4. The goal is to overcome NLOS situations by placing the RIS between transmitter and receiver such that an indirect link is created. This concept is depicted in Figure 2.1. An improvement in system performance with respect to different metrics, such as end-to-end SNR, is expected.

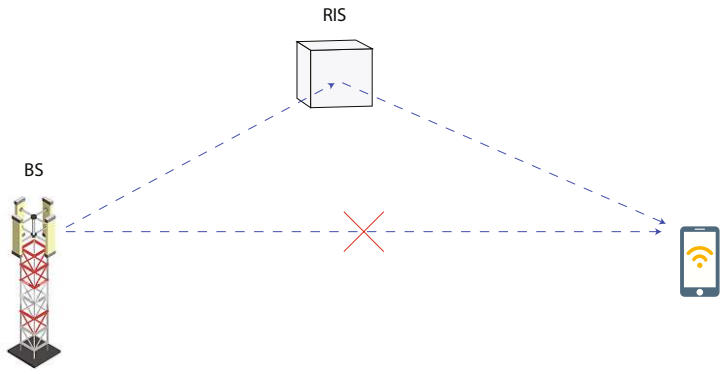

Figure 2.1: A RIS used as a reflector to overcome NLOS situations.

2.1.3 Lens

Scientists of NTT DOCOMO and AGC released an article on their website with an intelligent surface used as a lens [7], however technical details for this technology are currently unknown. According to their provided information, this might build a potential use case for railroad, while replacing windows with these surfaces to enhance the signal strength near seats. This is illustrated in Figure 2.2.

2.1.4 Enhancing physical layer security

Security is an omnipresent topic throughout wireless communications, especially because large portions of signals can be transmitted to an eavesdropper. Active and passive beamforming provides the freedom to focus signal power on desired users and simultaneously reduce this power on potential eavesdroppers. A figure of merit in physical layer security is the secrecy rate, which is the difference between the rate of the main communication channel and the maximum rate of the eavesdropper. This rate can be analyzed in RIS assisted wireless communication systems, as in [8] and [9]. Particularly in [8] is concluded, that it is more beneficial in terms of secrecy rate to deploy a large-scale RIS instead of increasing the number of transmit antennas at the

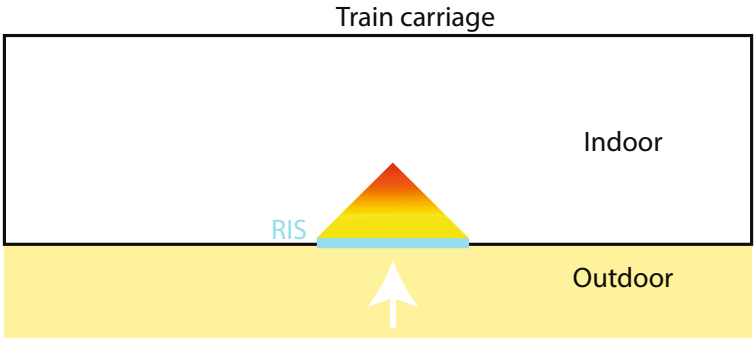

Figure 2.2: A RIS used as a lens to focus the electromagnetic wave in a train near seats. The RIS replaces the window.

base station. Under this consideration, a deployment of intelligent surfaces might be beneficial for railroad scenarios regardless of the performance boost. An illustration can be found in Figure 2.3.

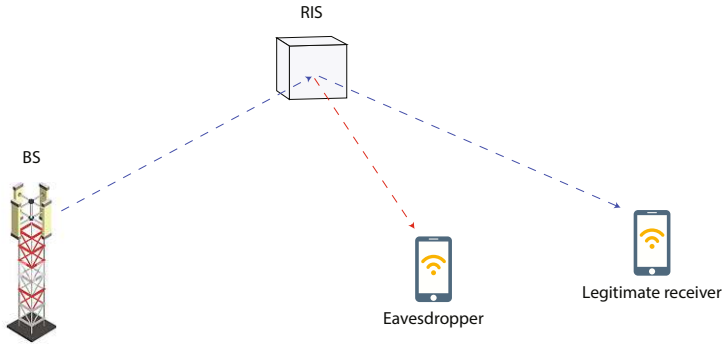

Figure 2.3: Enhancing physical layer security with a RIS.

2.2 STAR-RIS

In the previous section use cases for transmissive and reflective intelligent surfaces were discussed, however, there also exists an enhanced solution that combines both approaches, called Simultaneous Transmitting and Reflecting Reconfigurable Intelligent Surface (STAR-RIS). With this technology the elements can be partially reflective/-transmissive. Partial reflectivity means, that additionally to the reflection coefficient from the RIS elements a transmission coefficient is introduced into the system model. This promises a more versatile field of application especially when the transmission can be combined with the use case of a lens. Nevertheless, the design of such devices is more complex than the simpler RISs. An illustration of such design differences is

highlighted in [10] along with several use cases. Near and far field channel models for STAR-RISs are introduced in [11], but these models are not validated by measurements yet. Measurements of this technology are even rarer than the usual RIS, thus this topic might be more interesting when the investigation of both separate modes is further advanced.

2.3 Channel models

Developing simple but sufficiently accurate channel models for RISs is a challenging task. The evaluation of such models requires measurement campaigns and consequently available hardware. This is still an open topic and needs further clarification in the future, thus only a few sources for channel models are available. Generally speaking, channel models can be separated into statistical models using experimental data and models using the principle of geometry [12]. Intelligent surfaces are built around the concept of beamforming which often requires geometric information such that the geometric approach is reasonable for this technology. For this reason, a Rician geometric channel model as explained in Chapter 3 will be employed in this thesis. Similar approaches are used in [13] and [14].

2.4 Channel estimation

To fully achieve the performance gains brought by RISs the acquisition of accurate Channel State Information (CSI) is crucial, but practically challenging to obtain. The bare minimum of channel estimation which is required at the RIS is an angular estimation in order to determine the optimal phase shifts. This will be discussed in Chapter 3. Throughout this thesis, perfect channel knowledge at the receiver and RIS is assumed. In literature authors distinguish between semi-passive and (fully) passive RIS. The former is equipped with receive RF chains, whereas the latter is entirely passive. Due to the additional RF chains, pilots can be transmitted from either base station to RIS or from user to RIS. The additional sensing capability is less practical, but makes channel estimation easier. A detailed explanation on the topic of channel estimation for RISs can be found in [2]. Note that even a (fully) passive RIS cannot be without any sort of energy source due to the property of being electronically reconfigurable.

2.5 Currently available RIS technologies

This section provides a brief overview of the required hardware and manufacturing strategies to fabricate an intelligent surface. In order to provide a fair impression of the current state of research, the highlights of available measurement campaigns are concluded afterwards.

2.5.1 Structures

The reconfiguration of an intelligent surface can be done by several mechanisms. In particular electrical reconfiguration (voltage) might be the most common approach, however mechanical (stretching), thermal (thermal excitation) or optical reconfiguration (optical pump) are known alternatives [1]. The following paragraphs discuss the two possible structures of a RIS.

Metamaterial based RISs

According to [1] metamaterial based RISs or metasurfaces rely on the use of liquid crystals [15] or graphene [16]. According to [15], the approach with liquid crystals has severe problems with the reflection coefficient, where more than 60% is absorbed rather than reflected in simulations and measurements.

Patch-array based RISs

In this approach, a RIS is realized as a periodic collection of unit cells integrated on a substrate. Each cell is a subwavelength-sized element and can then be modeled by an equivalent electric circuit with a corresponding impedance. This impedance can be controlled for example with an electric voltage. In [17] varactor diodes were used for these cells with an equivalent series RLC circuit. A very similar approach with a slight difference in the equivalent circuit is used in [18].

2.5.2 Measurement campaigns

The quantity of available RISs is small and therefore not many real-world field trials exist, nevertheless it is utterly important to validate existing channel models with measurements. To the best of my knowledge, there are four intelligent surfaces available to academia, which will be discussed below. Note that companies in the industry such as NTT DOCOMO might also possess measurements, however they are not generally accessible as of yet.

In [19] near and far field measurements for three different RISs were done in an anechoic chamber. The near field measurements showed that the Path Loss (PL) is proportional to $(d_1 + d_2)^2$, where d_1 is the distance from the transmitter to the RIS and d_2 is the distance from the RIS to the receiver. This was validated with two different large surfaces for a carrier frequency of $10.5\,\text{GHz}$ with 10200 elements and 1700 elements, respectively. The far field measurement was done for one small RIS for $4.25\,\text{GHz}$ and 256 elements. In this setup, the path loss is proportional to $(d_1 d_2)^2$ with the same notation as before.

The authors of [17] have done indoor and outdoor field trials for a two state[1] RIS for 5.8 GHz with 1100 elements. The indoor test revealed a power gain of 26 dB, the 50 m outdoor test a 27 dB power gain and the 500 m outdoor test a 14 dB power gain while using the same device. What is causing this gain difference is not entirely clear from the study. Additionally Uplink (UL) and Downlink (DL) reciprocity for the Time Division Duplex (TDD) mode, which is commonly used in 5G communication systems, was validated. In this paper the reflection coefficient amplitude depending on the bias voltage got evaluated as further discussed in Section 3.5.3.

The BER is a common figure of merit, which will be further used in this thesis. In [20] this quantity was measured depending on either received SNR or transmit power for a 10 and 40 state RIS. This surface was designed with 256 elements for a carrier frequency of 4.25 GHz. The measurements were done in a 2×2 MIMO setup for a $16-$QAM modulation format.

Determining the power gain and radiation pattern was the goal of the measurements in [21]. These authors used a four state RIS consisting of 256 elements. With a 64-QAM modulation format a power gain of 21.7 dB and 19.1 dB could be observed for carrier frequencies of 2.3 GHz and 28.5 GHz, respectively.

[1] Note that the number of states refer to the number of possible quantized phase shifts of a RIS element.

3 Link level analysis

This chapter focuses on understanding the basic behaviour of the RIS in terms of link level simulations. This means, that most simulations will be done in terms of BER. At first, a geometric channel model will be introduced, such that this can also be used for the upcoming chapter, which focuses on system level simulations. A very important finding is how the phase shifts of the RIS should be determined, such that the most possible gain is obtained. The impact of different parameters from the channel model will be discussed. The analysis focuses on BER simulations mostly dependent on transmit power, but also K-factor, quantization step size and the number of RIS elements.
This chapter is designed with a NLOS link between transmitter and receiver in mind, which is connected to the system level analysis of the next chapter. Theoretically, this analysis can be interpreted as a detailed view of the system level analysis after the LOS to the base station is lost. To visualize this argument see Figure 3.1.
Notation: Matrices $\boldsymbol{A}$ and vectors $\boldsymbol{a}$ are described by upper and lower case bold symbols, respectively. The (i,j)th subscript refers to the ith row and jth column of a matrix $\boldsymbol{A}$ and is described by a_{ij}. The superscripts $\{\cdot\}^T$, $\{\cdot\}^*$, $\{\cdot\}^H$, $\{\cdot\}^{-1}$, represents the transpose, conjugate, conjugate transpose and the inverse of a matrix, respectively. A diagonal matrix is constructed under $\text{diag}\{\boldsymbol{a}\}$ with its diagonal elements described by the components of $\boldsymbol{a}$. The absolute value of x is given by $|x|$ and $||\cdot||_2$ is the l_2-norm. The element wise Hadamard product is described by $\odot$. A set is denoted by an upper case calligraphic symbol $\mathcal{B}$ with the corresponding cardinality $|\mathcal{B}|$. A complex Gaussian distribution with mean μ and variance σ^2 is represented by $\mathbb{C}\mathcal{N}(\mu,\sigma^2)$. $\mathbb{E}\{\cdot\}$ denotes the expectation operator and j is the imaginary unit.

3.1 Channel model

The basic transmission system can be seen in Figure 3.1, where the base station uses N_{Tx} transmit antennas, the RIS consists of N elements and the receiver has one omnidirectional receive antenna. I consider a two-dimensional scenario with a Uniform Linear Array (ULA) for both the antenna and RIS elements. Due to this assumption, beamforming in azimuth is sufficient. This model can be generalized to other array structures, that also support 3D-beamforming.
The received symbol at the user y can be written as

$$y = \boldsymbol{h}\boldsymbol{f}\sqrt{P_{Tx}}x + n \tag{1}$$

with the transmitted symbol $x \in \mathbb{C}^{1\times 1}$, the transmit power $P_{Tx} \in \mathbb{R}_+^{1\times 1}$, the channel vector[2] $\boldsymbol{h} \in \mathbb{C}^{1\times N_{Tx}}$, the precoding vector for beamforming $\boldsymbol{f} \in \mathbb{C}^{N_{Tx}\times 1}$ and the noise $n \sim \mathbb{C}\mathcal{N}(0,\sigma_n^2)$.

[2] An extension from the channel vector $\boldsymbol{h}$ to a channel matrix $\boldsymbol{H}$ is doable by increasing the number

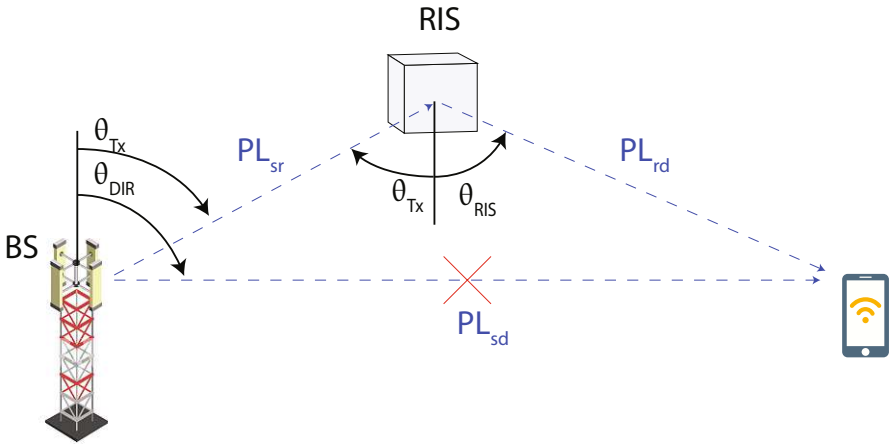

Figure 3.1: Scenario for the link level simulations including the required angles of departure/arrival.

Throughout this chapter it is assumed, that the path over the RIS will lead to better results, therefore the beamforming is done towards the RIS, i.e. the normalized precoding vector $\boldsymbol{f}$ is given by

$$\boldsymbol{f} = \frac{1}{\sqrt{N_{Tx}}} \boldsymbol{a_{BS}}(\theta_{Tx}) \tag{2}$$

with an array response vector $\boldsymbol{a_{BS}} \in \mathbb{C}^{N_{Tx} \times 1}$ of

$$\boldsymbol{a_{BS}}(\theta) = \left[1, \exp\left(j2\pi \frac{d}{\lambda} sin(\theta)\right), \ldots, \exp\left(j2\pi \frac{d}{\lambda} sin(\theta)(N_{Tx}-1)\right)\right]^T. \tag{3}$$

At the receiver I invert the effective channel, under the assumption of perfect channel knowledge, to estimate the transmit symbol x from the received symbol y. The detected symbol $\hat{x}$ can be calculated as

$$\hat{x} = \frac{1}{\boldsymbol{hf}\sqrt{P_{Tx}}} y. \tag{4}$$

The overall channel vector $\boldsymbol{h}$ consists of a direct path $\boldsymbol{g_{sd}} \in \mathbb{C}^{N_{Tx} \times 1}$ and a tandem channel over the RIS, i.e. a channel from base station to RIS $\boldsymbol{G_{sr}} \in \mathbb{C}^{N \times N_{Tx}}$, a RIS response matrix $\boldsymbol{\Phi} \in \mathbb{C}^{N \times N}$ and a channel from RIS to receiver $\boldsymbol{g_{rd}} \in \mathbb{C}^{N \times 1}$. Each of these parts is scaled by the square root of the path loss PL_{sd}, PL_{sr}, PL_{rd}, respectively. The channel vector is written as

of receive antennas from one to N_{Rx}. Note that the channel vector is the only vector which is defined as a row vector in order to keep the notation simpler.

$$\boldsymbol{h} = \boldsymbol{g_{rd}}^H \boldsymbol{\Phi} \boldsymbol{G_{sr}} \frac{1}{\sqrt{PL_{sr} PL_{rd}}} + \boldsymbol{g_{sd}}^H \frac{1}{\sqrt{PL_{sd}}}. \tag{5}$$

Note that the RIS is treated as a new addition to the environment, which adds additional power to the total received power. This is done in order to have a fair comparison against the base environment with an empty space in place of the RIS.
Each part of the channel is modeled as Rician with a geometric array response vector $\boldsymbol{a_{BS}}(\cdot)$ and/or $\boldsymbol{a_{RIS}}(\cdot)$. Note that $\boldsymbol{a_{RIS}} \in \mathbb{C}^{N \times 1}$ is defined similarly as in Equation (3) with different number of elements, i.e. N instead of N_{Tx}, to account for the response from the RIS instead of the BS. The components of the channel vector in Equation (5) are given by

$$\boldsymbol{g_{sd}} = \sqrt{\frac{K_{sd}}{1+K_{sd}}} \boldsymbol{a_{BS}}(\theta_{DIR}) + \sqrt{\frac{1}{1+K_{sd}}} \boldsymbol{h_r}, \quad \boldsymbol{h_r} \sim \mathbb{CN}\left(\boldsymbol{0}, \boldsymbol{I_{N_{Tx} \times N_{Tx}}} \sigma_h^2\right) \tag{6}$$

$$\boldsymbol{g_{rd}} = \sqrt{\frac{K_{rd}}{1+K_{rd}}} \boldsymbol{a_{RIS}}(\theta_{RIS}) + \sqrt{\frac{1}{1+K_{rd}}} \boldsymbol{g_r}, \quad \boldsymbol{g_r} \sim \mathbb{CN}\left(\boldsymbol{0}, \boldsymbol{I_{N \times N}} \sigma_h^2\right) \tag{7}$$

$$\boldsymbol{G_{sr}} = \sqrt{\frac{K_{sr}}{1+K_{sr}}} \boldsymbol{a_{RIS}}(\theta_{Tx}) \boldsymbol{a_{BS}}(\theta_{Tx})^H + \sqrt{\frac{1}{1+K_{sr}}} \boldsymbol{H_r}, \tag{8}$$

$$\boldsymbol{H_{r_i}} \sim \mathbb{CN}\left(\boldsymbol{0}, \boldsymbol{I_{N \times N}} \sigma_h^2\right) \tag{9}$$

where σ_h^2 denotes the variance of the diffuse channel. Each component has a corresponding K-factor, which is defined as a Rician K-factor and describes the power ratio between the specular components and the diffuse components.
The RIS response matrix $\boldsymbol{\Phi}$ has a diagonal shape under the assumption, that there is no coupling between the individual RIS elements. Considering the reflectivity α this matrix is given by

$$\boldsymbol{\Phi} = \alpha \cdot \mathrm{diag}(\boldsymbol{\varphi}), \tag{10}$$

with

$$\boldsymbol{\varphi} = \left[\exp(j\gamma_1), \ldots, \exp(j\gamma_N)\right]^T, \tag{11}$$

where $\boldsymbol{\varphi} \in \mathbb{C}^{N \times 1}$ contains the phase shifts of the individual RIS elements γ_i with $i = 1, \ldots, N$. Note that perfect reflection means $\alpha = 1$ which is assumed throughout this chapter unless stated otherwise.
According to [22] the optimum $\boldsymbol{\varphi}$, corresponding to optimal phase shifts in terms of power, can be obtained as

$$\boldsymbol{\varphi}_{opt} = \boldsymbol{a_{RIS}}(\theta_{RIS}) \odot \boldsymbol{a_{RIS}}^*(\theta_{Tx}). \tag{12}$$

3.2 Simulation setup

In this section the simulation setup and parameters will be discussed. The overall transmission system consists of a modulator, precoder, channel, receive filter and a demodulator as depicted in Figure 3.2. This transmission system is implemented in Matlab [4] in order to perform Monte-Carlo simulations with random channel realizations following the models introduced in Section 3.1.
For one iteration, the modulator maps K random bits from the dataword u to a complex valued transmit symbol x. The number of bits is dependent on the modulation format, for example, a 16-QAM modulation format requires $log_2(16) = 4$ bits. The transmit symbol x is scaled by the square root of the transmit power P_{Tx}. After the application of the precoder $\boldsymbol{f}$ and transmission over the channel $\boldsymbol{h}$, which adds a random realization of noise n, the received symbol y is scaled by the receive filter by $\frac{1}{\boldsymbol{hf}\sqrt{P_{Tx}}}$ to obtain the detected symbol $\hat{x}$. This symbol is demapped to the detected dataword $\hat{u}$ which is compared to the original dataword u. With many iterations over this transmission system the BER can be simulated. Note that this simple transmission system does not consider any coding, thus the number of data bits and code bits is equal. In other words the coding rate R is equal to one.

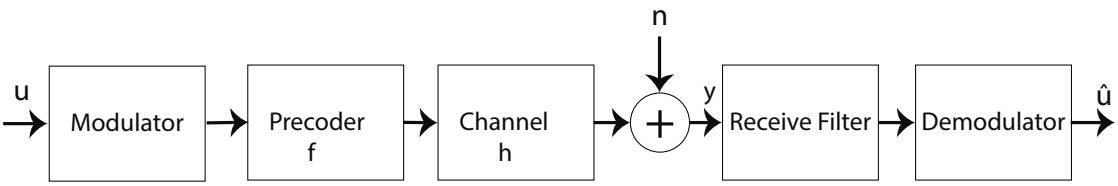

Figure 3.2: Simple transmission system for BER simulations.

A high-order symbol alphabet of 64-QAM is chosen, as a representation for a channel with high Channel Quality Indicator (CQI). The symbol alphabet order can be reduced for a channel with low CQI. The path loss of the direct link is set to be 50 dB higher than the path loss of the tandem link to account for NLOS between transmitter and receiver. The carrier frequency is based on available frequencies for railroads in Austria. The transmit and noise power are chosen based on available data from OpenRailwayMap [23], which will be explained in Chapter 4. The RIS and antenna element spacing is based on common uses in literature and the geometric parameters (angles) are chosen arbitrarily as they do not affect the observed behaviour. In Table 3.1 are the simulation parameter summarized. They stay the same for all simulations throughout this chapter unless stated otherwise.

QAM Order	64
Path loss Tx-RIS	60 dB
Path loss RIS-Rx	90 dB
Path loss Tx-Rx	200 dB
Carrier frequency	2.5 GHz
K_{sd}	10 dB
K_{sr}	20 dB
K_{rd}	20 dB

Transmit antennas	8
Receive antennas	1
Transmit power	$25 \dots 65$ dBm
Noise power	-85 dBm
Antenna spacing (BS)	$\frac{\lambda}{2}$
Element spacing (RIS)	$\frac{\lambda}{2}$
θ_{Tx}	$\frac{\pi}{4}$
θ_{RIS}	$\frac{\pi}{9}$

Table 3.1: Simulation parameters for the link level simulations.

3.3 Power scaling law

Beamforming appears when phase shifted copies of the same signal are emitted from multiple antennas. This leads to constructive and destructive interference at different locations as known from classical wave propagation. If the waves interfere constructively, then a so-called array gain can be observed and this array gain is the topic of this section.
A RIS can be considered as a passive beamformer, because it receives the signal from the base station and re-radiates it towards the receiver without having a dedicated energy source for amplification. In order to obtain constructive interference, a phase synchronization of the elements is required. Optimal synchronization is considered by optimal phase shifts within the RIS, whereas random, i.e. suboptimal, phase shifts still achieve a power gain as shown in the upcoming sections. This effect of a RIS on the system performance is considered as the power scaling law or square law, i.e. every doubling of the number of RIS elements N achieves about 6 dB power gain for optimized RIS phase shifts and about 3 dB for random phase shifts. Random phase shifts are considered uniformly distributed between 0 and 2π. Similar effects are observed in [24] and [25].

3.3.1 Optimal phase shifts

Optimal phase shifts are obtained by synchronizing the wavefronts at the receiver, i.e. introducing a phase shift in the RIS elements according to Equation (12). In Figure 3.3 the 6 dB power scaling for optimal phase shifts is shown as a simulation of BER over transmit power in dBm. Starting with the purple curve with 4 RIS elements, up to the dark blue curve with 64 elements.
A derivation of this 6 dB power gain for optimized phase shifts is done in the following. The linear receive SNR is given by

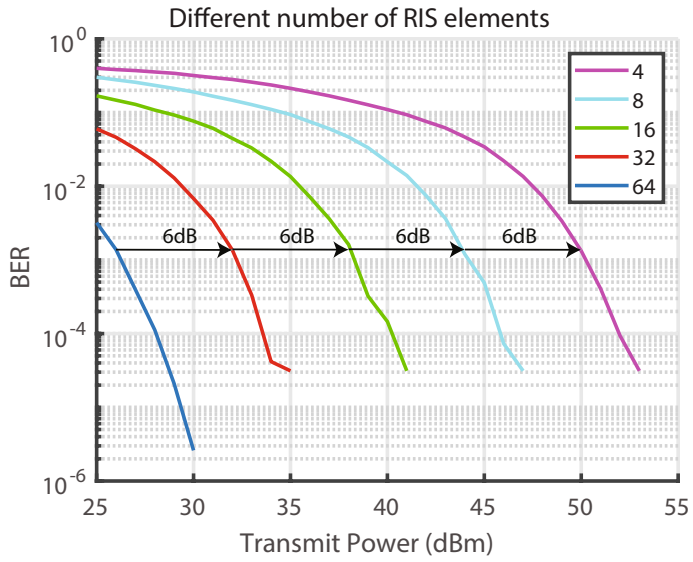

Figure 3.3: BER over transmit power in dBm for different number of RIS elements N and optimal phase shifts. Every doubling of N leads to a $6\,\mathrm{dB}$ gain.

$$SNR = \frac{|\boldsymbol{h}\boldsymbol{f}\sqrt{P_{Tx}}|^2}{\sigma_n^2} = \frac{|\boldsymbol{h}\boldsymbol{a}_{\boldsymbol{BS}}(\theta_{Tx})\sqrt{P_{Tx}}|^2}{\sigma_n^2 N_{Tx}}, \tag{13}$$

where in the last step the precoding vector $\boldsymbol{f}$ from Equation (2) was used. Inserting the channel vector $\boldsymbol{h}$ from Equation (5) leads to

$$SNR = \frac{P_{Tx}}{\sigma_n^2 N_{Tx}} \left| \boldsymbol{g_{rd}}^H \boldsymbol{\Phi} \boldsymbol{G_{sr}} \frac{1}{\sqrt{PL_{sr} PL_{rd}}} \boldsymbol{a}_{\boldsymbol{BS}}(\theta_{Tx}) + \boldsymbol{g_{sd}}^H \frac{1}{\sqrt{PL_{sd}}} \boldsymbol{a}_{\boldsymbol{BS}}(\theta_{Tx}) \right|^2. \tag{14}$$

With an infinite K-factor this $6\,\mathrm{dB}$ power gain is achieved, which simplifies the following derivation. Only the specular components of the channel in Equation (6)-(8) are relevant, because the diffuse components become zero for $K \to \infty$ due to the prefactor of $\frac{1}{1+K}$. With this knowledge the SNR can be simplified to

$$SNR = \frac{P_{Tx}}{\sigma_n^2 N_{Tx}} \cdot \left| \frac{\beta_{rd}\beta_{sr}}{\sqrt{PL_{sr} PL_{rd}}} \boldsymbol{a}_{\boldsymbol{RIS}}(\theta_{RIS})^H \boldsymbol{\Phi} \boldsymbol{a}_{\boldsymbol{RIS}}(\theta_{Tx}) \boldsymbol{a}_{\boldsymbol{BS}}(\theta_{Tx})^H \boldsymbol{a}_{\boldsymbol{BS}}(\theta_{Tx}) + \frac{\beta_{sd}}{\sqrt{PL_{sd}}} \boldsymbol{a}_{\boldsymbol{BS}}(\theta_{DIR})^H \boldsymbol{a}_{\boldsymbol{BS}}(\theta_{Tx}) \right|^2, \tag{15}$$

with

$$\beta_{sd} = \sqrt{\frac{K_{sd}}{1+K_{sd}}} \tag{16}$$

$$\beta_{rd} = \sqrt{\frac{K_{rd}}{1+K_{rd}}} \tag{17}$$

$$\beta_{sr} = \sqrt{\frac{K_{sr}}{1+K_{sr}}}. \tag{18}$$

Inserting Equation (12) in Equation (10) and consequently in Equation (15) matches the array response vectors onto each other and leads to

$$SNR = \frac{P_{Tx}}{\sigma_n^2 N_{Tx}} \left| \frac{\beta_{rd}\beta_{sr}\alpha}{\sqrt{PL_{sr}PL_{rd}}} N N_{Tx} + \frac{\beta_{sd}}{\sqrt{PL_{sd}}} \boldsymbol{a_{BS}}(\theta_{DIR})^H \boldsymbol{a_{BS}}(\theta_{Tx}) \right|^2. \tag{19}$$

The expression in Equation (19) is proportional to N^2 which explains the $6\,\text{dB}$ power gain for every doubling on the number of RIS elements.

3.3.2 Random phase shifts

The random phase shifts are obtained by a uniform distribution between 0 and 2π. Figure 3.4 shows the $3\,\text{dB}$ power gain for random phase shifts as a simulation of BER over transmit power in dBm.

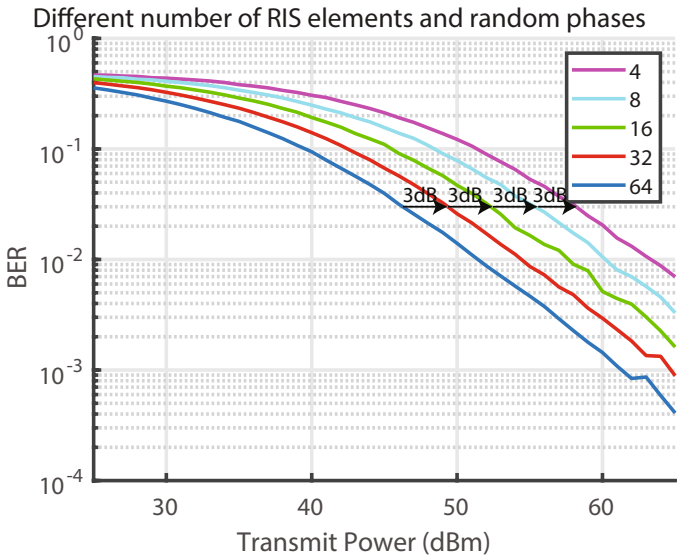

Figure 3.4: BER over transmit power in dBm for different number of RIS elements N and random phase shifts. Every doubling of N lead to a $3\,\text{dB}$ gain.

The $3\,\text{dB}$ gain can be explained by reconsidering Equation (14). The element response matrix $\mathbf{\Phi}$ for random phase shifts γ_i and $i = 1, \ldots, N$ is given by

$$\mathbf{\Phi} = \alpha \cdot \text{diag}\left(\exp\left(j\gamma_1\right), \ldots, \exp\left(j\gamma_N\right)\right). \tag{20}$$

The phase shifts γ_i are uniformly distributed in $[0, 2\pi)$. Calculating the expectation with respect to the random phase shifts can be formulated as

$$\mathbb{E}\left\{SNR\right\}, \tag{21}$$

where the SNR is given by Equation (14). The channel coefficients which do not cancel each other out are given by

$$\boldsymbol{\xi} = \boldsymbol{a_{RIS}}\left(\theta_{RIS}\right)^* \odot \boldsymbol{a_{RIS}}\left(\theta_{Tx}\right). \tag{22}$$

The following simplification can be done since all γ_i are zero mean and independent and identically distributed thus

$$\mathbb{E}\left\{\left|\sum_{i=1}^{N} \xi_i \exp\left(j\gamma_i\right)\right|^2\right\} = \sum_{i=1}^{N} \mathbb{E}\left\{\left|\xi_i \exp\left(j\gamma_i\right)\right|^2\right\} = N, \tag{23}$$

where ξ_i is the ith element of $\boldsymbol{\xi}$. Consequently, the expected SNR is proportional to N, as in

$$\mathbb{E}\left\{SNR\right\} \approx \frac{P_{Tx}}{\sigma_n^2 N_{Tx}} N. \tag{24}$$

This explains the $3\,\text{dB}$ power gain for doubling the number of RIS elements N.
Note that Figure 3.3 and Figure 3.4 have a different slope, thus a different diversity order. The effective channel in Figure 3.3 is AWGN for very large K-factors and thus has an infinite diversity order. This is beneficial in terms of reliability, as fading is minimal. Figure 3.4 has an effective channel which corresponds to Rayleigh fading. This is due to the fact, that each surface element has a product of two Gaussians multiplied by a random phase shift, which corresponds to double-Rayleigh fading. At the receiver the sum of these individual channels is observed thus this results in an effective Rayleigh fading channel for sufficiently large number of RIS elements.

3.4 Impact of the K-factor

A Rician channel model is often used in conjunction with a strong dominant component. This dominant component can be for instance the LOS wave and is also known as the specular or LOS component. The power ratio between the specular and the diffuse

component is called the Rician K-factor and provides an indication of link quality. This parameter is influenced by the multipath propagation environment. For example in a rural railway scenario, which is considered later in this thesis, one would mostly expect a large K-factor, because there is not too much scattering in the environment close to the receiver/train. In an urban environment a smaller K-factor would be more appropriate, as the density of scattering objects is higher.
In this section, the impact of the K-factors from the channel model, see Equation (6)-(8), is considered. Until now it was unclear how the magnitude of the K-factors changes the performance in terms of BER. Additionally, the importance of the three different K-factors, i.e. K_{sd}, K_{sr} and K_{rd}, will be investigated, because in a NLOS scenario the direct link with the corresponding K_{sd} will be different as the indirect link.

Simulation parameters

The simulation parameters are the same as in Table 3.1 with the difference that K_{sd}, K_{sr} and K_{rd} are variable.

3.4.1 Optimal phase shifts

This is a first look at the order of magnitude of the K-factors considering optimal phase shifts from Equation (12). I want to emphasize, that the derivation of the optimal phase shifts are based on the assumption of an infinite K-factor. Consequently, the result of Equation (12) is only optimal, if the K-factor is sufficiently large, thus beamforming is done entirely over the specular component. If the K-factor is not large enough, the optimal solution could be found by beamforming over the effective channel, i.e. the sum of the specular and diffuse component. However, to keep track of the diffuse channel by channel estimation is difficult for high mobility scenarios such as railroad, because the channel changes very quickly. For these simulations all K-Factors, i.e. K_{sd}, K_{sr} and K_{rd}, are varied simultaneously. From the orange up to the red curve, in Figure 3.5, the K-factors are varied from $0\,$dB up to $20\,$dB, with a possible power gain of up to $7\,$dB. These curves have the same slope, which means that for a large K-factor we end up with an effective AWGN channel. In contrary, the cyan, grey and green curve represent low K-factors with a different slope. This slope represents a Rayleigh fading channel.

3.4.2 Optimal phase shifts with partial LOS

This section focuses on understanding the impact of K-factors, especially with a disappearing LOS. This will be important in the next chapter, as the LOS will change to NLOS in the direct link at some point. One or more K-factors will be varied in a range

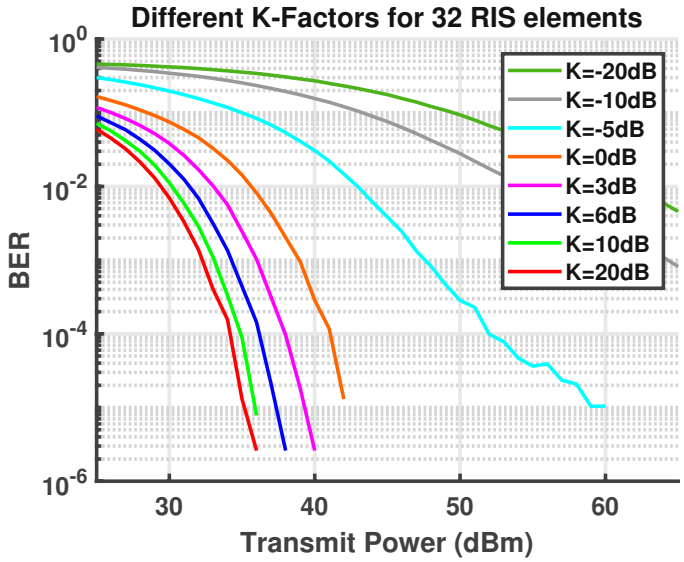

Figure 3.5: BER over transmit power in dBm for 32 RIS elements and different K-factors.

from 0 dB up to 40 dB, which is sufficient to cover all relevant cases in the upcoming chapter.
Figure 3.6 analyzes the impact of the three different K-factors. As a reference, the cyan curve shows the case where all three are scaled simultaneously. The blue curve, while two out of three possible K-factors are varied, behaves similarly to the cyan curve with $K_{sd} = 10$ dB, therefore K_{sd} does not impact the system performance under the assumption of high path loss, i.e. a blocked LOS. In the red and green curve K_{sr} and K_{rd} are altered respectively, while the other remaining K-factors are fixed. A performance gain is observable, because one part of the tandem channel already has LOS, contrary to the cyan curve, where no LOS is given at the start.
To further emphasize the importance of the K-factor, additional simulations of BER over transmit power are depicted in Figure 3.7. All green curves are done for a K_{sr} of 20 dB, while K_{rd} is varied from -10 dB up to 10 dB. In the red curves, K_{sr} and K_{rd} are altered in an identical fashion. Note that the green curve with the square markers has a different slope than the red curve with the dot markers. Comparing these two curves highlights, that it is more important to have both links with an acceptable K-factor, rather than having one link with a high and one link with a low K-factor.
In summary both K-factors K_{sr} and K_{rd} should be in an acceptable range, to have a better performance in terms of BER. This should be satisfied in a railroad scenario, because it only makes sense to place a RIS with LOS to both endpoints. The impact of the K-factor on the direct link K_{sd} is minor, as the path loss on this link is high.

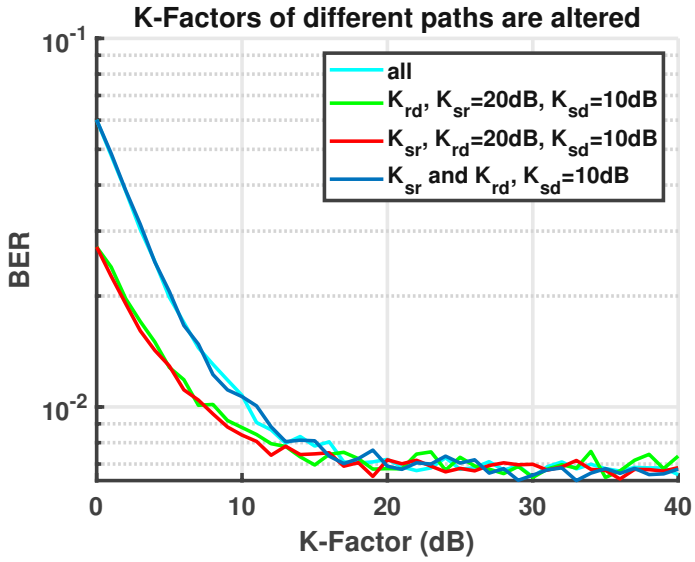

Figure 3.6: BER over K-factor for different paths and 32 RIS elements.

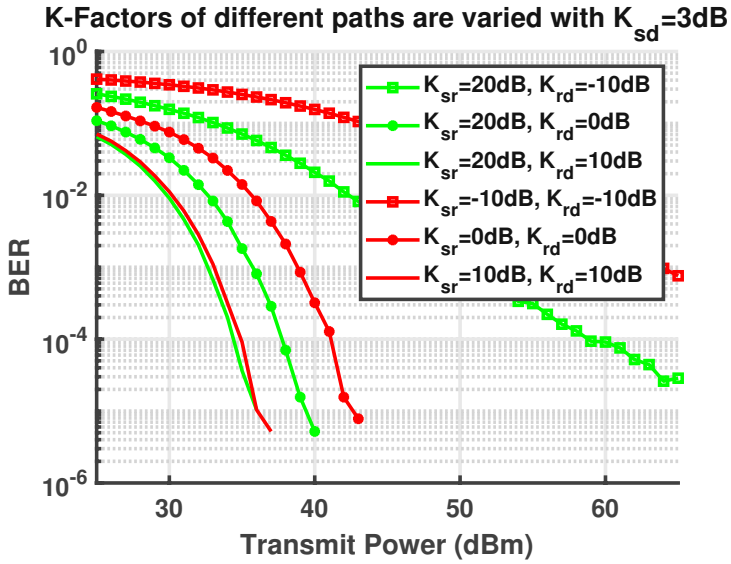

Figure 3.7: BER over transmit power in dBm for different paths and 32 RIS elements.

3.5 Impact of non-optimality

So far perfect reflective RIS elements with a continuous set of phase shifts were used. These assumptions only hold true for a close to perfect RIS. Currently available surfaces, especially in the early stages of research, might not fit these requirements, therefore it is useful to look into the impact of non-optimality.
This section analyzes the system performance degradation with respect to non-optimal RIS elements. Firstly, the impact of quantized phase steps is considered for different step sizes. Secondly, a random phase distortion, due to imperfect angular estimation, is evaluated. Thirdly, the assumption of perfect reflection is dropped, i.e. $\alpha \neq 1$ in Equation (10), such that the impact of different reflectivity is discussed.

3.5.1 Quantized phase shifts

Using a RIS with continuous phase shifts might be advantageous in terms of pure performance, but the downside is the cost, because the manufacturing of such precise elements requires sophisticated design and expensive hardware. The simplest approach would be to consider only a two-level or two-state[3] phase shift, i.e. 0 or π. This approach is also considered in [25]. In order to obtain more insight into this whole quantization topic, several stages of quantization are considered in the following.
Figure 3.8 shows the impact of quantized phase shifts compared to a continuous phase shift in terms of BER over transmit power simulations. The possible phase shifts depend on the quantization step size, e.g. a stepsize of $\frac{\pi}{2}$ corresponds to the possible phases of $\left[0, \frac{\pi}{2}, \pi, 3\frac{\pi}{2}\right]$. This quantization can be seen in the red curve. Reducing the number of possible phase shifts from continuous to a four-step quantization is a major difference in angles with only a slight impact on the system performance. The quantization step size of $\frac{\pi}{4}$ is already very close to the continuous phase shift, as seen in the green curve.

3.5.2 Random phase distortion

In order to obtain the optimal phase shifts as considered in Equation (12) the angles θ_{RIS} and θ_{Tx} have to be known at the RIS. As the angular estimation might not always be perfect, a random phase distortion on top of these two angles is considered. The phase distortion θ_{dist} is given by a Gaussian distribution $\mathcal{N}\left(0, \sigma_p^2\right)$. This consideration changes φ_{opt} to

$$\boldsymbol{\varphi}_{dist} = \boldsymbol{a_{RIS}}\left(\theta_{RIS} + \theta_{dist}\right) \odot \boldsymbol{a_{RIS}}^{*}\left(\theta_{Tx} + \theta_{dist}\right). \tag{25}$$

Figure 3.9 shows the impact of such a distortion for different variances σ_p^2. Even a small variance of phase distortion like $\frac{\pi}{512}$, as depicted in the grey curve, already

[3] In literature the number of states is also classified by bits b. For example, a two-state RIS would equal one bit, because the number of phase shift levels L is given by $L = 2^b$.

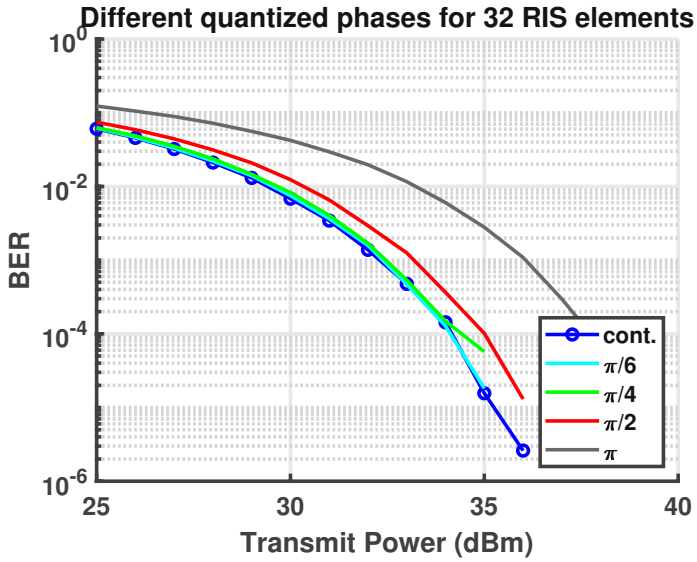

Figure 3.8: BER over transmit power in dBm for different quantized phase shifts.

changes the BER behaviour drastically. Note that the phase distortion also changes the slope of the BER curves. I want to emphasize, that the phase distortion is added two times in Equation (25) thus the overall RIS phase distortion has double the variance. Additionally, the magnitude of the distortion is the square root of the variance, e.g. a phase distortion variance of $\frac{\pi}{512}$ results in an error magnitude of around ± 4.5 degree.

3.5.3 Impact of the reflectivity

Lossless and non frequency-selective reflectivity is an omnipresent assumption in most existing RIS literature, however there are already different dependencies known for a RIS. In this section different dependencies are discussed from available literature sources. Starting with a frequency dependency, followed by a change in reflectivity based on the phase shift of the elements. As a last point, simulations for the NLOS scenario with constant, but imperfect reflectivity are discussed.

Frequency dependency

In [17] a RIS was designed where a unit cell consists of two varactor diodes. The goal was to create a two-state RIS, with phases 180 degree apart from each other. Simulations were done based on the equivalent RLC series circuit before the RIS was built. These simulations show the reflection coefficient and reflected phase based on the control voltage, see Figure 3.10. Due to the fact, that the impedance of the RLC circuit is frequency dependent, also the response changes with frequency. The authors

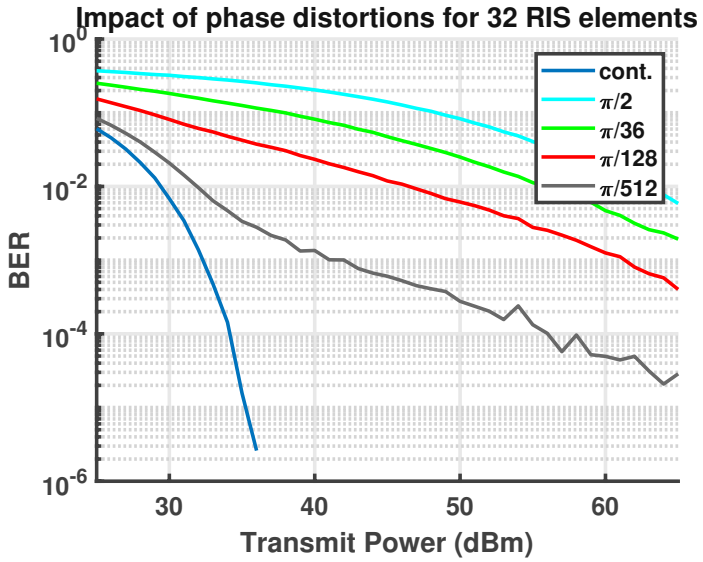

Figure 3.9: BER over transmit power in dBm for different phase distortion variance σ_p^2.

of the paper chose to design a RIS for $5.8\,\text{GHz}$ and at this frequency two control voltages of, for example $7\,\text{V}$ and $16\,\text{V}$ could be used. Looking at Figure 3.10 for the $16\,\text{V}$ curve and a $5.8\,\text{GHz}$ system with a bandwidth of $400\,\text{MHz}$, would result in a reflection amplitude of around 0.7 and 0.95 for the respective ends of the spectrum. These simulations already suggest, that it might become difficult to design a RIS for several frequencies simultaneously, which limits the versatility of these devices.

Phase shift dependency

The authors of [26] have modelled a RIS by an equivalent circuit similar to [17]. The modelling was done slightly different, by adding a parallel impedance to the RLC series circuit. According to their simulations, the amplitude of the reflection coefficient is dependent on the phase shift of the element itself, this behaviour is shown in Figure 3.11, where v_n is the n-th component of the diagonal matrix $\mathbf{\Phi}$ in Equation (10). The effective resistance R_n, in their equivalent circuit, determines the amount of power dissipation due to losses. This is a design parameter for a RIS element which cannot be zero in practice, but should be as low as possible.
A similar behaviour was observed in the previously discussed surface from [17] where measurements based on the designed RIS have shown, that the control voltages has to be $3.8\,\text{V}$ and $16\,\text{V}$ to achieve the 180 degree phase difference. The gain fluctuations of their measurement are around $6.5\,\text{dB}$, as seen in Figure 3.12. This would result in a reflection coefficient of $\alpha = 1$ for $16\,\text{V}$ and $\alpha = 0.22$ for $3.8\,\text{V}$.

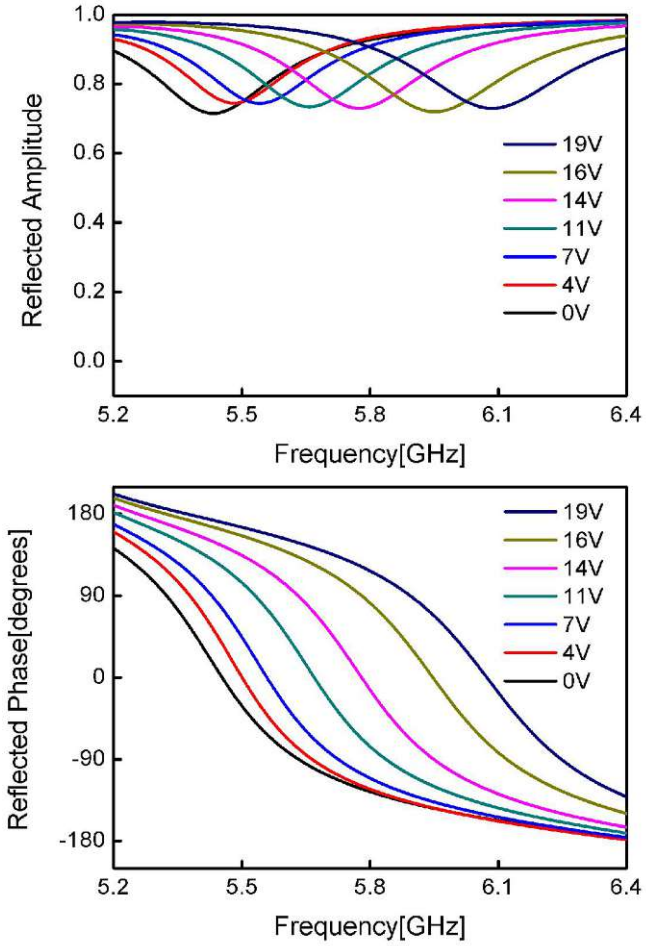

Figure 3.10: Modelled frequency dependency of the reflectivity for different control voltages. Source: [17, Figure 3] licensed under CC BY 4.0.

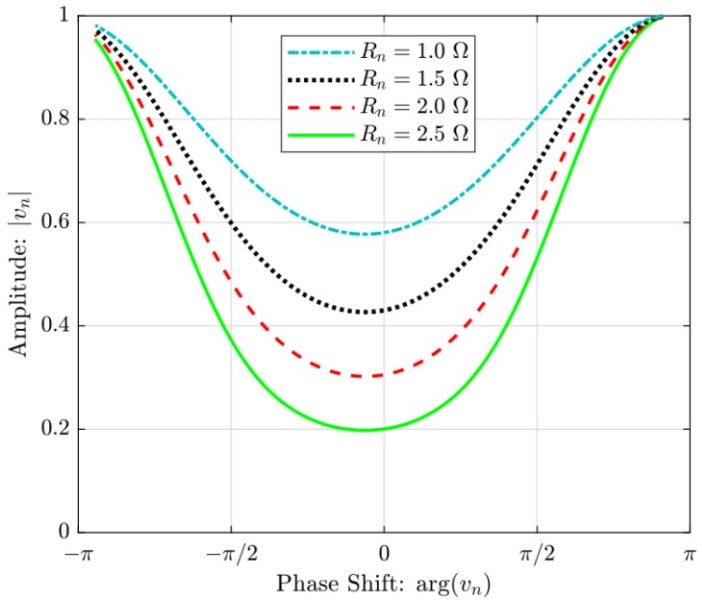

Figure 3.11: Magnitude of the reflection coefficient over the phase shift of a RIS element for different modelling parameters. Source: [26, Figure 3] ©2020 IEEE.

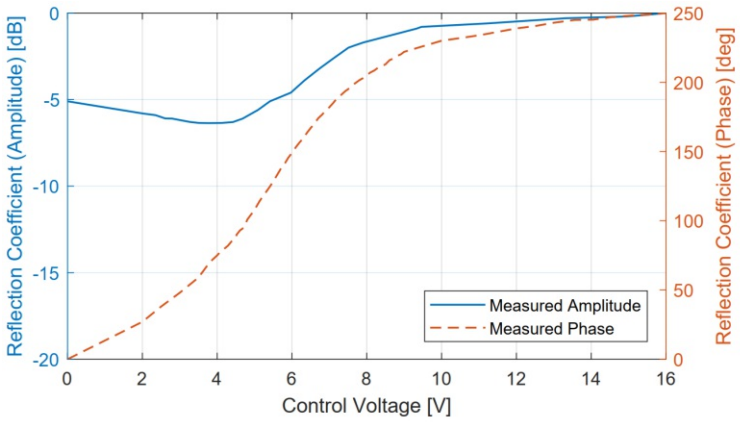

Figure 3.12: Measured reflection amplitude of a RIS over control voltage for 5.8 GHz. Source: [17, Figure 9] licensed under CC BY 4.0.

Constant reflectivity

In order to obtain a realistic impression of different reflectivity on the NLOS scenario a non frequency-selective, but lossy reflectivity is assumed. This means the reflection coefficient is decremented from 100% to 10% in steps of 10% in the link level simulations.
The impact of the different reflection coefficient α can be seen in Figure 3.13 in terms of BER over transmit power simulations. At high reflectivity a $10\,\%$ loss equals approximately a $1\,$dB power loss. This rule of thumb changes heavily for reflectivity below $50\,\%$.

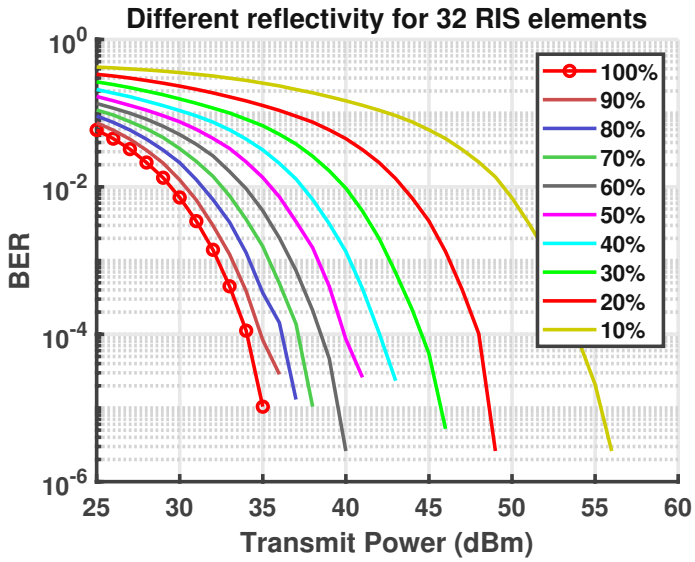

Figure 3.13: BER over transmit power in dBm for different reflectivity.

For every specific simulation setup the impact of reflectivity can be calculated analytically and is done in the following steps. The linear SNR is given by

$$SNR = \frac{|\boldsymbol{h}\boldsymbol{f}\sqrt{P_{Tx}}|^2}{\sigma_n^2}. \tag{26}$$

The channel with a general reflection coefficient α can be simplified to

$$\boldsymbol{h}\,(\alpha) = \boldsymbol{g}_{rd}^H \alpha \boldsymbol{\Phi} \boldsymbol{G}_{\boldsymbol{sr}} \frac{1}{\sqrt{PL_{sr}PL_{rd}}} + \boldsymbol{g}_{sd}^H \frac{1}{\sqrt{PL_{sd}}} = \alpha \boldsymbol{h_1} + \boldsymbol{h_2}. \tag{27}$$

The linear SNR reduction can be expressed as the quotient with perfect reflectivity, i.e. $\alpha = 1$, and a generally reduced reflectivity α by

$$\frac{SNR}{\hat{SNR}} = \frac{\frac{|\boldsymbol{h}(1)\boldsymbol{f}|^2\sqrt{P_{Tx}}}{\sigma_n^2}}{\frac{|\hat{\boldsymbol{h}}(\alpha)\boldsymbol{f}|^2\sqrt{P_{Tx}}}{\sigma_n^2}} = \frac{|\boldsymbol{h}\,(1)\,\boldsymbol{f}|^2}{|\hat{\boldsymbol{h}}\,(\alpha)\,\boldsymbol{f}|^2} = \frac{|\boldsymbol{h_1 f} + \boldsymbol{h_2 f}|^2}{|\alpha \boldsymbol{h_1 f} + \boldsymbol{h_2 f}|^2} = \tag{28}$$

$$= \frac{(\boldsymbol{h_1 f} + \boldsymbol{h_2 f})(\boldsymbol{h_1 f} + \boldsymbol{h_2 f})^H}{(\alpha \boldsymbol{h_1 f} + \boldsymbol{h_2 f})(\alpha \boldsymbol{h_1 f} + \boldsymbol{h_2 f})^H} = \tag{29}$$

$$= \frac{\boldsymbol{h_1 f f^H h_1^H} + \left(\boldsymbol{h_2 f f^H h_1^H} + \boldsymbol{h_1 f f^H h_2^H}\right) + \boldsymbol{h_2 f f^H h_2^H}}{\alpha^2 \boldsymbol{h_1 f f^H h_1^H} + \alpha\left(\boldsymbol{h_2 f f^H h_1^H} + \boldsymbol{h_1 f f^H h_2^H}\right) + \boldsymbol{h_2 f f^H h_2^H}}. \tag{30}$$

In the last step of Equation (28) the product for complex numbers with its conjugate, i.e. $ZZ^* = |Z|^2$, was used.
In order to solve this problem analytically, the Rayleigh fading part of $\boldsymbol{h_1}$ and $\boldsymbol{h_2}$ are considered as random variables. The expected SNR reduction becomes

$$\frac{\mathbb{E}\{SNR\}}{\mathbb{E}\{\hat{SNR}\}} = \frac{\mathbb{E}\{\boldsymbol{h_1 f f^H h_1^H} + \left(\boldsymbol{h_2 f f^H h_1^H} + \boldsymbol{h_1 f f^H h_2^H}\right) + \boldsymbol{h_2 f f^H h_2^H}\}}{\mathbb{E}\{\alpha^2 \boldsymbol{h_1 f f^H h_1^H} + \alpha\left(\boldsymbol{h_2 f f^H h_1^H} + \boldsymbol{h_1 f f^H h_2^H}\right) + \boldsymbol{h_2 f f^H h_2^H}\}}. \tag{31}$$

With the expectation operator each term can be simplified to

$$\mathbb{E}\{\boldsymbol{h_1 f f^H h_1^H}\} = \frac{\beta_{rd}^2 \beta_{sr}^2}{PL_{sr} PL_{rd}} \cdot$$
$$\boldsymbol{a_{RIS}}\,(\theta_{RIS})^H\, \boldsymbol{\Phi a_{RIS}}\,(\theta_{Tx})\, \boldsymbol{a_{BS}}\,(\theta_{Tx})^H\, \boldsymbol{f f^H a_{BS}}\,(\theta_{Tx})\, \boldsymbol{a_{RIS}}\,(\theta_{Tx})^H\, \boldsymbol{\Phi}^H \boldsymbol{a_{RIS}}\,(\theta_{RIS}) \tag{32}$$

$$\mathbb{E}\{\boldsymbol{h_1 f f^H h_2^H}\} = \frac{\beta_{rd}\beta_{sr}\beta_{sd}}{\sqrt{PL_{sr} PL_{rd} PL_{sd}}} \cdot$$
$$\boldsymbol{a_{RIS}}\,(\theta_{RIS})^H\, \boldsymbol{\Phi a_{RIS}}\,(\theta_{Tx})\, \boldsymbol{a_{BS}}\,(\theta_{Tx})^H\, \boldsymbol{f f^H a_{BS}}\,(\theta_{DIR}) \tag{33}$$

$$\mathbb{E}\{\boldsymbol{h_2 f f^H h_1^H}\} = \frac{\beta_{rd}\beta_{sr}\beta_{sd}}{\sqrt{PL_{sr} PL_{rd} PL_{sd}}} \cdot$$
$$\boldsymbol{a_{BS}}\,(\theta_{DIR})^H\, \boldsymbol{f f^H a_{BS}}\,(\theta_{Tx})\, \boldsymbol{a_{RIS}}\,(\theta_{Tx})^H\, \boldsymbol{\Phi}^H \boldsymbol{a_{RIS}}\,(\theta_{RIS}) \tag{34}$$

$$\mathbb{E}\{\boldsymbol{h_2 f f^H h_2^H}\} = \frac{\beta_{sd}^2}{PL_{sd}} \boldsymbol{a_{BS}}\,(\theta_{DIR})^H\, \boldsymbol{f f^H a_{BS}}\,(\theta_{DIR}) \tag{35}$$

with

$$\beta_{sr} = \sqrt{\frac{K_{sr}}{1 + K_{sr}}} \tag{36}$$

$$\beta_{rd} = \sqrt{\frac{K_{rd}}{1 + K_{rd}}} \tag{37}$$

$$\beta_{sd} = \sqrt{\frac{K_{sd}}{1 + K_{sd}}}. \tag{38}$$

Note that Equation (31) can further be simplified by inserting the precoding vector $\boldsymbol{f}$ from Equation (2). This will show the quadratic dependence on the number of RIS elements N similar to Equation (19).
The SNR loss can be calculated analytically dependent on the reflectivity and the remaining parameters, which are given in Table 3.1. Table 3.2 summarizes this behaviour for 32 RIS elements.

α in %	SNR loss in dB
90	0.915
80	1.938
70	3.098
60	4.437
50	6.020
40	7.957
30	10.455
20	13.972
10	19.965

Table 3.2: Reduced receive SNR depending on reflectivity for 32 RIS elements.

3.6 Distributed antenna system compared with a RIS

A Distributed Antenna System (DAS) is a network of spatially separated antenna nodes, where one is called a Remote Radio Unit (RRU). All of those RRUs are connected to the Base Band Unit (BBU), which does all the necessary signal processing, such as generating the transmit symbols and calculating the beamformers. Note that the connection between the RRUs and the BBU is done with a fibre, which significantly increases the deployment costs compared to placing a RIS. A DAS is a potential candidate for 6G technology similar to RISs. For this reason, it is of interest to compare an intelligent surface with such a system. Specifically, this means that the simulation scenario as in Figure 3.1 is reconsidered. For the DAS the RIS will be replaced by a RRU with variable transmit power, whereas the existing RRU has constant power, see Figure 3.14. A comparison of these two setups is difficult, because introducing a new RRU for the railway means, that additional transmit power at RRU_2 will be consumed. Additionally, the geometric setup should stay the same as in the case of the intelligent surface simulations in order to get a fair comparison. This specifically means, that the path loss PL_{Tx1Rx} is $200\,\text{dB}$, whereas the path loss PL_{Tx2Rx} is $90\,\text{dB}$. Scaling the transmit power from the first RRU, which is done for the RIS simulation setup, only marginally changes the system performance. This would result in a flat BER over receive SNR or transmit power curve. A solution to this problem can be found by

scaling the transmit power of the second RRU, however this RRU is way closer to the receiver, thus needs significantly less transmit power compared to the RIS simulation setup.

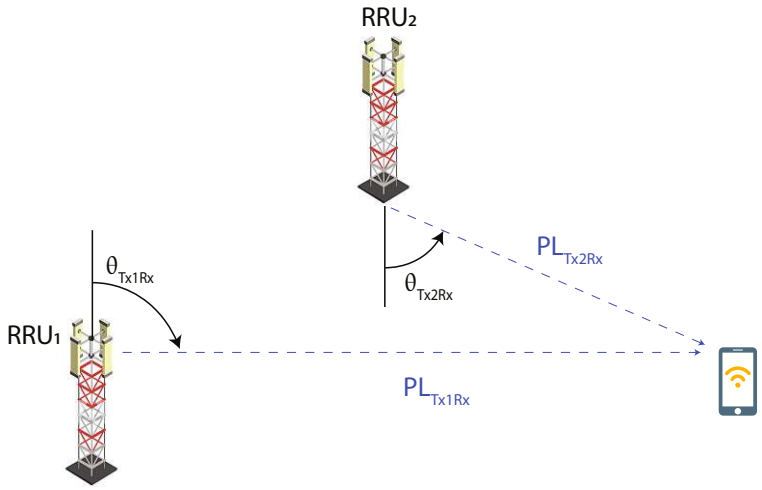

Figure 3.14: Scenario for the DAS including the corresponding angles of departure and path loss.

3.6.1 Channel model for the DAS

In section 3.1 the channel model for the RIS simulations was discussed. For the DAS the model has to be adapted. The received symbol $y \in \mathbb{C}^{1\times 1}$ at the user with one omnidirectional receive antenna is given by

$$y = \boldsymbol{h_1 f_1}\sqrt{P_{RRU1}}x + \boldsymbol{h_2 f_2}\sqrt{P_{RRU2}}x + n \tag{39}$$

with the transmitted symbol $x \in \mathbb{C}^{1\times 1}$, the transmit powers $P_{RRU1}, P_{RRU2} \in \mathbb{R}_{+}^{1\times 1}$, the channel vectors $\boldsymbol{h_1}, \boldsymbol{h_2} \in \mathbb{C}^{1\times N_{Tx}}$, the precoding vectors for beamforming $\boldsymbol{f_1}, \boldsymbol{f_2} \in \mathbb{C}^{N_{Tx}\times 1}$ and the noise $n \sim \mathbb{C}\mathcal{N}(0, \sigma_n^2)$. The subscript 2 refers to the newly placed RRU instead of the RIS. For a DAS the beamforming is done directly to the user such that the precoding vectors $\boldsymbol{f_1}, \boldsymbol{f_2}$ are defined similar to Equation (2) for different angles θ_{Tx1Rx}, θ_{Tx2Rx} and are given by

$$\boldsymbol{f_1} = \frac{1}{\sqrt{N_{Tx}}}\boldsymbol{a_{BS}}(\theta_{Tx1Rx}) \tag{40}$$

$$\boldsymbol{f_2} = \frac{1}{\sqrt{N_{Tx}}}\boldsymbol{a_{BS}}(\theta_{Tx2Rx}). \tag{41}$$

Note that $\boldsymbol{a_{BS}}(\theta)$ is used in order to have a consistent notation, although in a DAS the transmitting units are called RRUs instead of base stations.

The channel vector is defined as Rician channel vector equally to Equation (6). The detected symbol can finally be obtained by

$$\hat{x} = \frac{1}{\boldsymbol{h_1 f_1}\sqrt{P_{RRU1}} + \boldsymbol{h_2 f_2}\sqrt{P_{RRU2}}} y. \tag{42}$$

3.6.2 Simulation results

In the introduction to the topic of the DAS the problem of a fair comparison, due to the different path loss, was highlighted. This means that in case of the RIS simulation setup the transmit power has to be significantly higher for a small number of RIS elements, than the transmit power in case of the DAS simulations. However, a special case for a very large number of RIS elements, i.e. $N = 1024$, is also considered, which reduces the required transmit power. A summary of the simulation parameters can be found in Table 3.3.
In Figure 3.15 the BER over transmit power for different number of RIS elements is shown. In the blue curve for $N = 1024$ the transmit power range was reduced to $0 \ldots 20$ dBm. Due to the increased computational complexity, for this amount of RIS elements, the number of iterations was reduced as well. In summary a RIS assisted wireless network can be competitive with a DAS, as long as the number of RIS elements is large and the number of antennas at the RRUs is small.
Note that the path loss of the link between RRU_1 and the receiver is so high, that RRU_1 could be turned off, without changing the performance in terms of BER significantly. Consequently, the transmit power of RRU_1 is not included in the x-axis of Figure 3.15.

QAM Order	64
Path loss Tx1-Rx	200 dB
Path loss Tx2-Rx	90 dB
Carrier frequency	2.5 GHz
K_{Tx1Rx}	10 dB
K_{Tx2Rx}	20 dB
θ_{Tx1Tx2}	$\frac{\pi}{4}$
θ_{Tx2Rx}	$\frac{\pi}{9}$

Transmit antennas RRU_1	8
Transmit antennas RRU_2	8
Transmit antennas (RIS scenario)	8
Receive antennas	1
Transmit power (DAS) RRU_1	10 dBm
Transmit power (DAS) RRU_2	$0 \ldots 20$ dBm
Transmit power (RIS scenario)	$0 \ldots 45$ dBm
Noise power	-85 dBm
Antenna spacing	$\frac{\lambda}{2}$

Table 3.3: Simulation parameters for the DAS.

3.7 Summary of most important findings

This chapter provided an overview of how a RIS performs in terms of link level simulations. Starting with the power scaling law, i.e. every doubling of the number of RIS

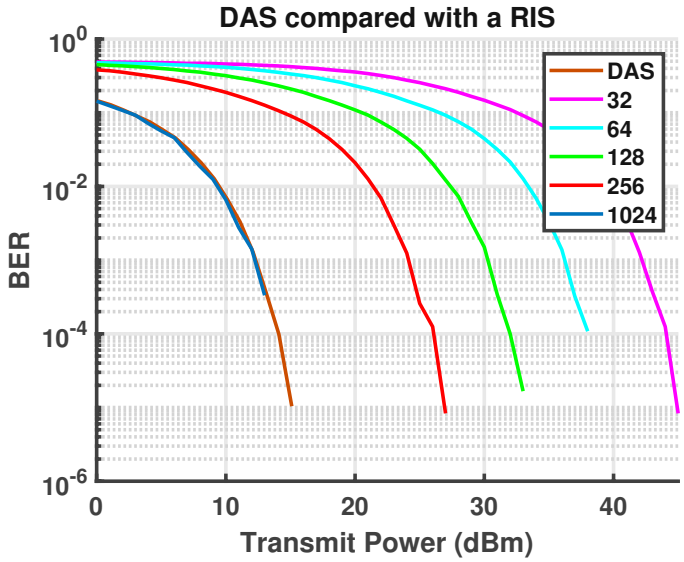

Figure 3.15: BER over transmit power in dBm for the DAS and RIS simulation setup. Different number of RIS elements N are considered.

elements achieves about $6\,$dB power gain for optimized RIS phase shifts. A smaller gain was also visible for randomized phase shifts with a uniform distribution between 0 and 2π.
The analysis continued with the impact of the K-factor, which revealed that the performance is better if both K-factors of the indirect link are moderate, rather than one K-factor is high and one is low. The K-factor has an additional impact on the slope of the BER over transmit power curve. This slope indicates the diversity order, thus is a measure of reliability.
The early research state of this technology comes with the problem of currently imperfect intelligent surfaces, which means that the common literature assumptions of non-frequency selective reflectivity and a continuous set of phase shifts might not be realistic. For this reason, the impact of these imperfections was discussed. A quantization of the phase states showed a minor degradation of the system performance, i.e. decreasing the set of phase states from continuous to four led to a power loss of around $1\,$dB. The reflectivity was a more complex topic, as there are several dependencies observed throughout literature. First of all, the frequency dependency of the reflection coefficient makes the design of surfaces for a moderate bandwidth difficult. A major problem for the RISs is the phase shift dependency. This means in particular, that the amplitude of the reflection coefficient is dependent on the phase shift, which should be introduced by the RIS. A reflectivity loss of up to 78% was observed in literature. Consequently, link level simulations for a reduced reflection coefficient were done. These simulations revealed that a reflectivity loss of 10% equals a power loss of

around 1 dB for reflectivity above 50%.
Last but not least an alternative to intelligent surfaces in railroad, i.e. distributed antenna systems, was discussed. Both technologies are potential candidates for 6G wireless communication systems, however a comparison of these systems is difficult. On the one hand, a DAS always requires a base station and consequently external transmit power with additional operational costs. On the other hand, a RIS is passive and comes only with the investment costs. Simulations showed that both technologies are competitive despite the difference in power allocation.

4 System level analysis

Using a fixed Modulation and Coding Scheme (MCS) as in Chapter 3 was helpful for the link level simulations, especially to show the different slope of the BER curves. However, this is not really relevant for practical systems, as the the MCS would be adapted to the channel conditions [27], i.e. the receive SNR. Consequently the receive SNR provides more information than the BER for a realistic system. In this chapter, the performance impact of a RIS in terms of system level simulations will be analyzed. The goal of this discussion is to provide a realistic environment and consequently get an overview of how a RIS performs, if it has to serve an entire area, as depicted in Figure 4.1. Different placement strategies will be evaluated and several problematic key points are highlighted. The last few sections provide a setup of a RIS for railroad, which results in a performance gain.

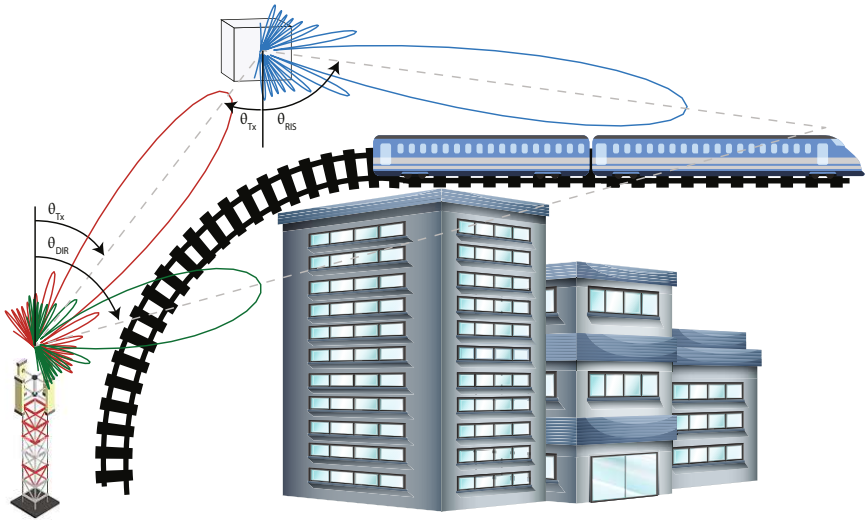

Figure 4.1: Illustration of the railroad scenario.

The channel model is the same as explained in Section 3.1. This model is dependent on the path loss and K-factor amongst other things, but these two parameters are especially difficult to determine without a measurement campaign based on the simulation scenario. Regarding this, a detailed explanation can be found in the following subsections. Throughout this chapter, perfect reflection and a continuous set of possible phase shifts are assumed.

4.1 Scenario geometry

Until now it was not necessary to introduce geometric parameters for the scenario, as the path loss and angles were fixed for the link level simulations. The introduction of such parameters was intentionally avoided in order to keep the link level analysis as general as possible. The varying angles and distances considered in this chapter raise the necessity to introduce an underlying geometry, which is basically the introduction of a coordinate system into Figure 4.1 as depicted in Figure 4.2. This specific geometry is based on a real-world railroad scenario taken from OpenRailwayMap [23]. OpenRailwayMap is an online map for the railway infrastructure throughout the World and free of charge. It is built on data from OpenStreetMap, which serves a similar purpose for vehicular communications and is open source as well. The real-world scenario can be seen in Figure 4.3. It is located in Austria, more precisely in Lower Austria, near Pottenbrunn and part of the (New) Western Railway. According to OpenRailwayMap the maximum velocity in this specific location is limited to $250\,\text{km/h}$, which fits in the path loss model requirements as explained in Section 4.2. Even tough this chapter considers movement as snapshot simulations along the tracks, the considered channel model from Section 3.1 does not consider Doppler-induced microscopic fading. To make this more clear, the channel model does not account for microscopic fading due to Doppler-shifts of the signal.
The blue line in Figure 4.2 shows the tracks of the railway, which are modeled as

$$y_{Train} = 275 - 275 \exp\left(-\frac{1}{100} x_{Train}\right) \tag{43}$$

where y_{Train} and x_{Train} are the corresponding coordinates of the train in meter. The black area shows a blockage, that blocks the LOS between the tracks and the base station around the origin. The orange line separates the visible LOS from the NLOS region from the perspective of the base station. Above this curve a visible LOS is guaranteed. The base station is placed at $y_{BS} = -8$ and $x_{BS} = -8$ in order to meet the minimum distance requirements of the path loss models in Section 4.2.

4.2 Path loss models

In order to have a standard compliant environment the 3rd Generation Partnership Project (3GPP) path loss models from TR 38.901 v16.1.0 [28] are used. All of these models are valid for a frequency range from 0.5 to $100\,\text{GHz}$ and a mobile speed up to $500\,\text{km/h}$. The relevant models in a railway scenario are Rural Macro (RMa) and Urban Macro (UMa) for the rural and urban case, respectively. Additional restrictions to these models are given in Table 4.1. Both models have a LOS and NLOS parameterization simultaneously, as in Table 4.2. Both parameterizations are required as there is no disappearing LOS measurement campaign for railroad scenarios available in literature.

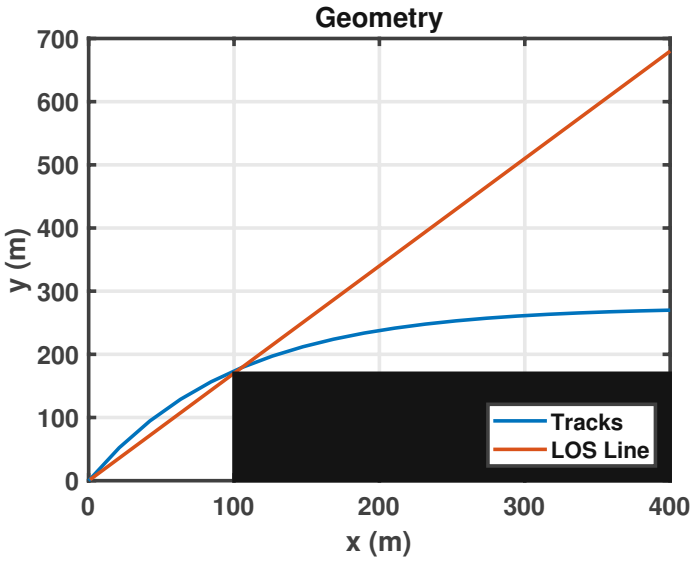

Figure 4.2: Geometry for the system level simulations.

Figure 4.3: Real world railroad scenario from OpenRailwayMap[23] near Pottenbrunn.

The average building height h and average street width W are difficult to determine in a railroad scenario, therefore the suggested default values from the report are used, i.e. $W = 20\,\text{m}$ and $h = 5\,\text{m}$. The models in Table 4.2 require a minimal two-dimensional distance of at least $10\,\text{m}$, which is considered by the base station and RIS placement.

	Rural Macro (RMa) LOS and NLOS	Urban Macro (UMa) LOS and NLOS
average building height h	$5 \ldots 50\,\text{m}$	\
average street width W	$5 \ldots 50\,\text{m}$	\
average base station height h_{BS}	$10 \ldots 150\,\text{m}$	\
average user terminal height h_{UT}	$1 \ldots 10\,\text{m}$	$1.5 \ldots 22.5\,\text{m}$

Table 4.1: Restrictions of RMa and UMA path loss models. Source: TR 38.901 v16.1.0 [28].

	Rural Macro (RMa)
LOS	$PL_{RMa-LOS} = \begin{cases} PL_1 & 10\,\text{m} \leq d_{2D} \leq d_{BP} \\ PL_2 & d_{BP} \leq d_{2D} \leq 10\,\text{km} \end{cases}$ $PL_1 = 20\log_{10}(40\pi d_{3D} f_c/3) + \min(0.03h^{1.72}, 10)\log_{10}(d_{3D})$ $-\min(0.044h^{1.72}, 14.77) + 0.002\log_{10}(h)\, d_{3D}$ $PL_2 = PL_1(d_{BP}) + 40\log_{10}(d_{3D}/d_{BP})$
NLOS	$PL_{RMa-NLOS} = \max\left(PL_{RMa-LOS}, \hat{PL}_{RMa-NLOS}\right)$ for $10\,\text{m} \leq d_{2D} \leq 5\,\text{km}$ $\hat{PL}_{RMa-NLOS} = 161.04 - 7.1\log_{10}(W) + 7.5\log_{10}(h)$ $-\left(24.37 - 3.7\,(h/h_{BS})^2\right)\log_{10}(h_{BS}) + (43.42 - 3.1\log_{10}(h_{BS}))(\log_{10}(d_{3D}) - 3)$ $+20\log_{10}(f_c) - \left(3.2\,(\log_{10}(11.75h_{UT}))^2 - 4.97\right)$
	Urban Macro (UMa)
LOS	$PL_{UMa-LOS} = \begin{cases} PL_1 & 10\,\text{m} \leq d_{2D} \leq \hat{d}_{BP} \\ PL_2 & \hat{d}_{BP} \leq d_{2D} \leq 5\,\text{km} \end{cases}$ $PL_1 = 28 + 22\log_{10}(d_{3D}) + 20\log_{10}(f_c)$ $PL_2 = 28 + 40\log_{10}(d_{3D}) + 20\log_{10}(f_c) - 9\log_{10}\left(\hat{d}_{BP}^2 + (h_{BS} - h_{UT})^2\right)$
NLOS	$PL_{UMa-NLOS} = \max\left(PL_{UMa-LOS}, \hat{PL}_{UMa-NLOS}\right)$ for $10\,\text{m} \leq d_{2D} \leq 5\,\text{km}$ $\hat{PL}_{UMa-NLOS} = 13.54 + 39.08\log_{10}(d_{3D}) + 20\log_{10}(f_c) - 0.6\,(h_{UT} - 1.5)$
	Additional Information
	$d_{BP} = 2\pi h_{BS} h_{UT} f_c/c_0, \quad c_0 = 3 \times 10^8\,\text{m/s}$ $\hat{d}_{BP} = 4\hat{h}_{BS}\hat{h}_{UT} f_c/c_0, \quad \hat{h}_{BS} = h_{BS} - 1, \quad \hat{h}_{UT} = h_{UT} - 1$ $d_{3D} = \sqrt{d_{2D}^2 + (h_{BS} - h_{UT})^2}$

Table 4.2: RMa and UMA path loss models with path loss in dB, carrier frequency in GHz and distances/heights in meters. Source: TR 38.901 v16.1.0 [28].

All possible path loss configurations of Table 4.2 are shown in Figure 4.4 and in Figure 4.5 with an exemplary RIS position of $x_{RIS} = 90$ and $y_{RIS} = 180$. Generally speaking, the path loss of NLOS links is higher than the path loss of LOS links. The gap between LOS and NLOS is way higher in the UMa case than in the RMa case. In the latter case, they only differ upon reaching a certain breakpoint distance as seen in Figure 4.4. Other than that, RMa and UMa with LOS behave very similarly.

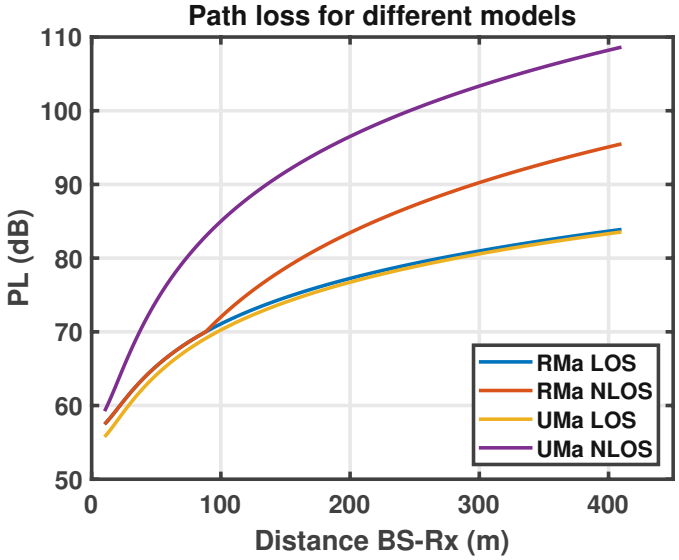

Figure 4.4: Path loss comparison for RMa and UMa models with LOS and NLOS, respectively.

Figure 4.5(a) up to Figure 4.5(d) depicts the path loss for the rural and urban models for the LOS and NLOS case, simultaneously. Due to the fact, that neither the base station nor the RIS is moving, the PL between Tx and RIS is always constant. As soon as the moving train/user is involved, the path loss varies over the distance. The purple curve in all four plots, i.e. the indirect link Tx-RIS-Rx, is just the sum of the orange and yellow curve. Due to the considered movement of the train, the distance between the RIS and the train becomes smaller until $210\,\text{m}$, where it rises again. This explains the dip in the RIS-Rx and consequently Tx-RIS-Rx curves. Additionally, a first impression of the orders of magnitude for path loss can be seen. A very important property of the path loss is, that in the used configuration the absolute minimum path loss, for the minimum distance of $10\,\text{m}$, is $55.95\,\text{dB}$. This means that even if the RIS is placed as close as possible to the tracks there is still a high path loss which has to be compensated with the RIS beamforming gain. Figure 4.5(d) is a plot for the relation between train location on the x-axis and distance between the base station and user.

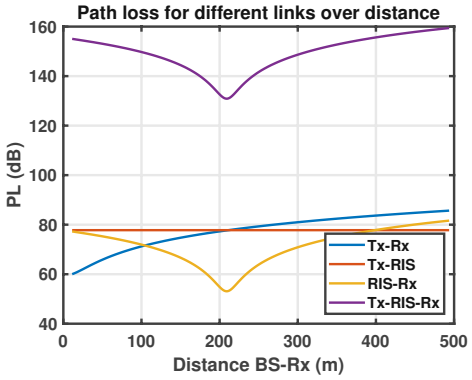

4.5(a): RMa LOS.

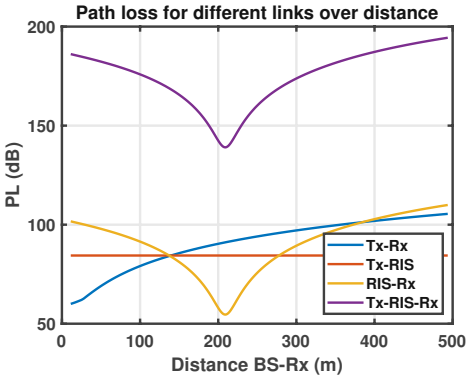

4.5(b): RMa NLOS.

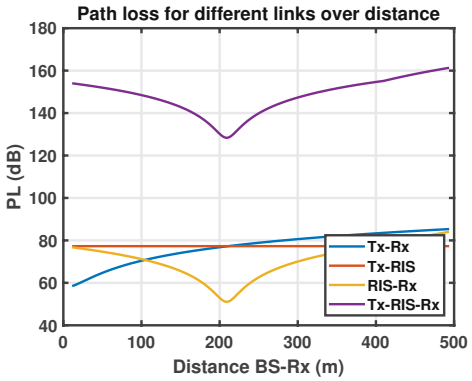

4.5(c): UMa LOS.

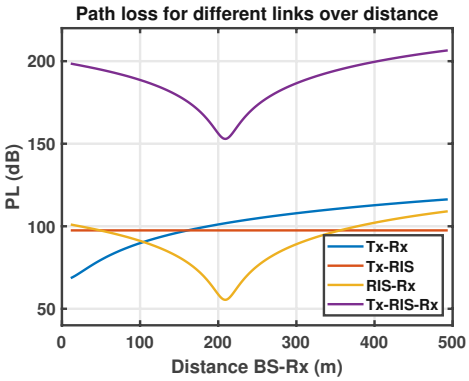

4.5(d): UMa NLOS.

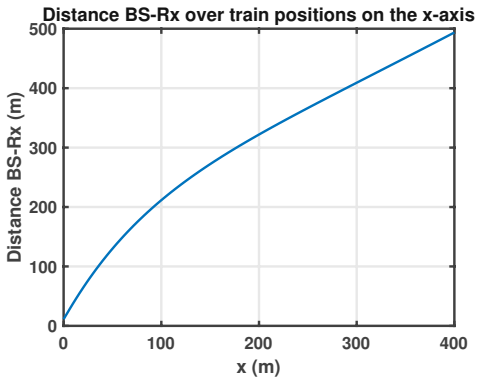

4.5(e): Relation between train position on the x-axis and distance BS-Rx.

Figure 4.5: Path loss for all possible configurations and an exemplary RIS position. Additionally, the relation between train position and distance BS-Rx is depicted.

4.3 K-factor models

As the geometric dimensions in a railway scenario are large, the intuition would suggest, that the K-factor might be distance dependent like the path loss. A possible parameterization for a distance dependent K-factor can be found in [29] for a carrier frequency of $930\,\text{MHz}$ and a viaduct railway scenario. The K-factor variation over the distance in this paper is really small and a constant K-factor seems like a good approximation. The constant assumption is also done in [30] for a carrier frequency of $100\,\text{GHz}$. Carefully note that the K-factor is approximated as a constant in the aforementioned sources, but they highly differ in their magnitude as frequency has a huge impact on the K-factor. Considering this frequency dependence, from now on the K-factor is approximated as a constant and set to $30\,\text{dB}$ in the LOS case, which is reasonable in a railway scenario up to $400\,\text{m}$ according to [31].

4.4 Determining an appropriate RIS position

The RIS position is an important topic as it has a direct influence on the path loss and other properties which determine the system performance. The placement has to be done for a specific criterion. In literature there exist some different approaches, where three of them are described in the following. Note that all of the discussed criteria are heuristics. Throughout this section indirect beamforming for the placement strategies is assumed.

4.4.1 Minimize path loss

A deterministic approach to obtain the RIS position could be done by minimizing the path loss. This has the advantage that this computation is very fast, in contrast the maximization of the received SNR or rate which require additional averaging. For a given set of possible railway positions $\mathcal{R}_{Train}$ and feasible RIS positions $\mathcal{R}_{RIS}$ the minimization could be formulated as

$$\min_{\boldsymbol{r_{RIS}}\in\mathcal{R}_{RIS}} \frac{1}{|\mathcal{R}_{Train}|} \sum_{\boldsymbol{r_{Train}}\in\mathcal{R}_{Train}} PL_{TxRISRx}\left(\boldsymbol{r_{RIS}}, \boldsymbol{r_{Train}}\right), \tag{44}$$

where $\boldsymbol{r_{RIS}} \in \mathbb{R}^2$ is the current RIS position, $\boldsymbol{r_{Train}} \in \mathbb{R}^2$ is the current position of the train, $PL_{TxRISRx}$ is the path loss over the indirect path.The set of all possible train positions is a reformulation of Equation (43) and is given by

$$\mathcal{R}_{Train} = \left\{ \boldsymbol{r_{Train}} \in \mathbb{R}^2 \,|\, y_{Train} = 275 - 275\exp\left(-\frac{1}{100}x_{Train}\right) \right\}. \tag{45}$$

Right now it is not clear how the set of all feasible RIS positions $\mathcal{R}_{RIS}$ should be defined and is intentionally avoided as this needs some further insight in the upcoming analysis.

4.4.2 Maximize average receive SNR

A common measure for placing a RIS is the end-to-end SNR as considered in [32]. The instantaneous SNR includes the random component of the channel and to determine this figure of merit averaging has to be performed. After determining the linear average received SNR SNR_{Rx} the RIS could be placed based on this information, such that the received SNR is maximized over the train positions. This can be formulated as

$$\max_{\boldsymbol{r_{RIS}} \in \mathcal{R}_{RIS}} \frac{1}{|\mathcal{R}_{Train}|} \sum_{\boldsymbol{r_{Train}} \in \mathcal{R}_{Train}} SNR_{Rx}\left(\boldsymbol{r_{RIS}}, \boldsymbol{r_{Train}}\right). \tag{46}$$

4.4.3 Maximize rate

Another common measure for the placement of wireless assisting devices such as RISs or relays is the rate [33]. This criterion is obtained by changing the argument of the maximization to the rate and can be formulated as

$$\max_{\boldsymbol{r_{RIS}} \in \mathcal{R}_{RIS}} \frac{1}{|\mathcal{R}_{Train}|} \sum_{\boldsymbol{r_{Train}} \in \mathcal{R}_{Train}} \log_2\left(1 + SNR_{Rx}\left(\boldsymbol{r_{RIS}}, \boldsymbol{r_{Train}}\right)\right). \tag{47}$$

4.4.4 Feasible RIS positions

Until now it was not stated how the set of all feasible RIS positions $\mathcal{R}_{RIS}$ is determined. Taking a look at Figure 4.6 we can see some feasible and infeasible areas for the RIS placement. The orange area is infeasible as it has no LOS to all possible track positions. In a similar fashion, the green area is also infeasible as it has no LOS to the base station. The pink area has LOS to the base station and to all possible track positions thus this area is part of $\mathcal{R}_{RIS}$. Remains the blue area, which requires an adaption on the defined angles for the channel model, as this only makes sense if a rotation of the RIS in azimuth is introduced.
Without such an adaption the set of feasible RIS positions $\mathcal{R}_{RIS}$ for the pink area can be described as

$$\mathcal{R}_{RIS} = \left\{\boldsymbol{r_{RIS}} \in \mathbb{R}^2 \,|\, y_{RIS} > 275 \,\text{and}\, y_{RIS} > y_{LOS}(x_{RIS}) \,\text{and}\, d_{RISRx} > 10\right\}, \tag{48}$$

with the LOS line given by

$$y_{LOS}(x) = \frac{17}{10}x. \tag{49}$$

A minimum distance between RIS and receiver of $10\,\text{m}$ is required to satisfy the restriction of the path loss models, see Table 4.2, such that

$$d_{RISRx} = \min_{\boldsymbol{r_{Train}} \in \mathcal{R}_{Train}} ||\boldsymbol{r_{RIS}} - \boldsymbol{r_{Train}}||_2. \tag{50}$$

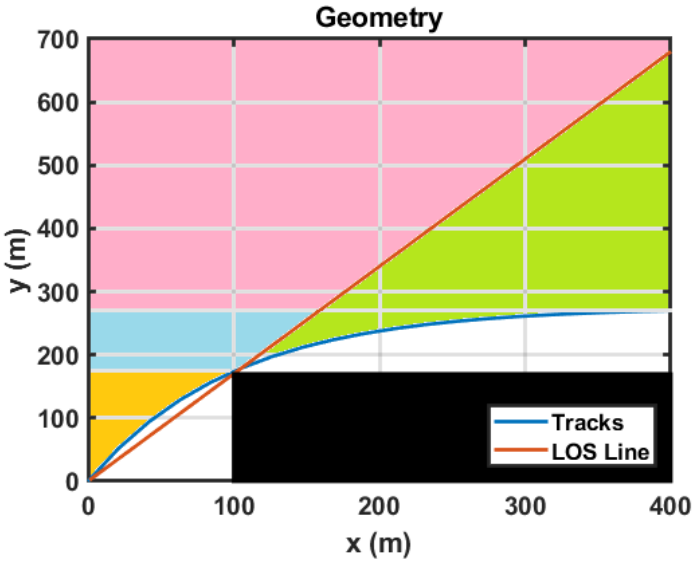

Figure 4.6: Geometry for the system level simulations with feasible RIS positions.

Including the blue area from Figure 4.6 this changes to

$$\mathcal{R}_{RIS} = \left\{ \boldsymbol{r_{RIS}} \in \mathbb{R}^2 \,|\, y_{RIS} > 170 \,\text{and}\, y_{RIS} > y_{LOS}(x_{RIS}) \,\text{and}\, d_{RISRx} > 10 \right\}. \quad (51)$$

In order to actually perform the calculations from Equation (44), (46) or (47) the sets of track and feasible RIS positions has to be discretized.

4.4.5 A required adaption to the angles in the channel model

As already mentioned in the previous section, the angles of the channel model have to be adapted, such that the RIS allows for a rotation in azimuth. This enables to include the blue area from Figure 4.6 into the calculation of the RIS positions. Concretely speaking the array response vectors of the RIS $\boldsymbol{a_{RIS}}(\theta_{RIS})$ and $\boldsymbol{a_{RIS}}(\theta_{Tx})$ in Equation (7), (8) and consequently (12) have to be replaced by

$$\boldsymbol{a_{RIS}}(\theta_{RIS} - \theta_0) \quad (52)$$

$$\boldsymbol{a_{RIS}}(\theta_{Tx} + \theta_0) \quad (53)$$

where θ_0 is the angle of the rotation from the y-axis towards the receiver, similar to θ_{RIS}. θ_0 has to be chosen, such that θ_{RIS} is smaller than $\frac{\pi}{2}$. For the underlying geometry $\theta_0 = \frac{\pi}{4}$ is a proper choice.

4.4.6 Heuristic RIS position for the RMa PL model

Until now three possible heuristic criteria and their necessary requirements were introduced such that a heuristic RIS position can be determined for a specific simulation

setup and path loss model. Right now there could be RIS positions calculated for the RMa and UMa path loss model in the variations of LOS and NLOS. A practical interesting setup is to use the RMa LOS case as the RIS might improve the system performance in a rural area by outperforming the base station regardless of the LOS between the BS and RIS. The used simulation parameter can be seen in Table 4.3.

Carrier frequency	2.5 GHz
K_{sd}	30 dB
K_{sr}	30 dB
K_{rd}	30 dB
θ_0	$\frac{\pi}{4}$

Transmit antennas	16
Receive antennas	1
Number of RIS elements	100
Transmit power	20 dBm
Noise power	−85 dBm
Antenna spacing (BS)	$\frac{\lambda}{2}$
Element spacing (RIS)	$\frac{\lambda}{2}$

Table 4.3: Simulation parameters for the heuristic RIS position with the RMa PL model and LOS.

In Figure 4.7 you can see the three heuristically determined positions for the RIS, which were calculated numerically. Intuitively one would say, that maximizing the rate and maximizing the average received SNR should be the same, as they are related via the $log_2(\cdot)$, but the rate has a summation afterward, which changes this behavior. In Table 4.4 are the final RIS positions.

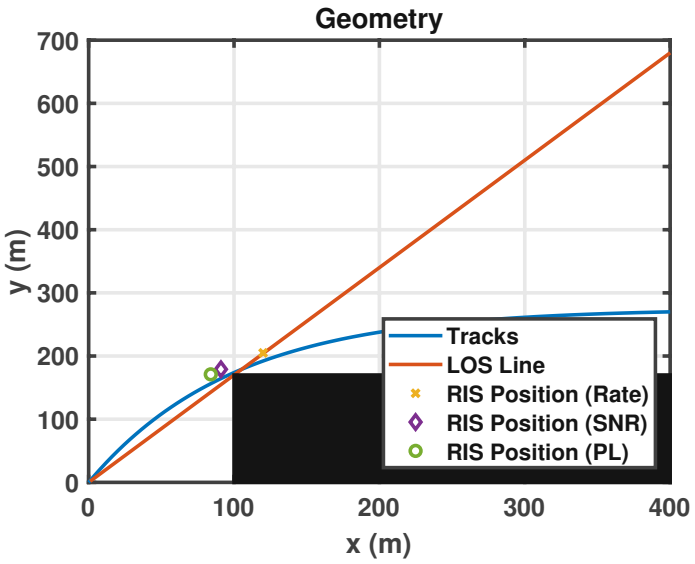

Figure 4.7: Heuristic RIS position for the RMa PL model and LOS.

A comparison of the three results in terms of system level simulations can be found in Figure 4.8. The locations of the path loss minimization and average receive SNR

Criteria	Position in meter as (x, y)
Minimum path loss	$(84, 171)$
Maximum avg. received SNR	$(91, 179)$
Maximum rate	$(120, 205)$

Table 4.4: Heuristic RIS positions for the RMa PL model and LOS.

maximization are very close in Figure 4.7, similar to the performance seen in the red and green curve in Figure 4.8. The black curve represents the rate maximization. Figure 4.8 shows some local minima of the SNR, where the black curve only has two of them, compared to the remaining two curves. These minima are due to destructive interference between the direct and indirect link.

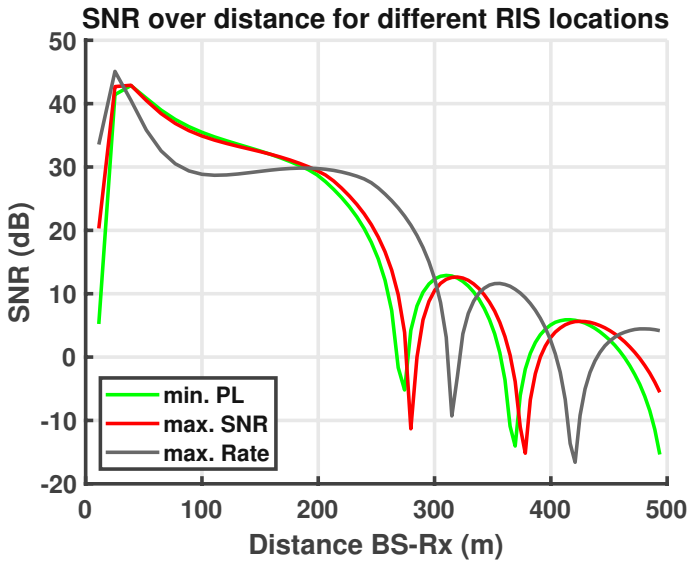

Figure 4.8: SNR over distance for the RMa LOS PL model and indirect beamforming.

Figure 4.9 compares the three different locations in terms of rate over distance. The green and red curve represent the minimization of path loss and maximization of the average received SNR, respectively. As already explained above, the distance between these two results is very small and so is the performance considered somewhat equal. The black curve represents the maximization of the rate. Due to the condition of maximizing the rate along the whole path, it is difficult to see if this holds true, thus the average-rate is calculated in Table 4.5 for the three different schemes.
For the remainder of this chapter the rate maximization criterion will be considered as the best placement strategy.

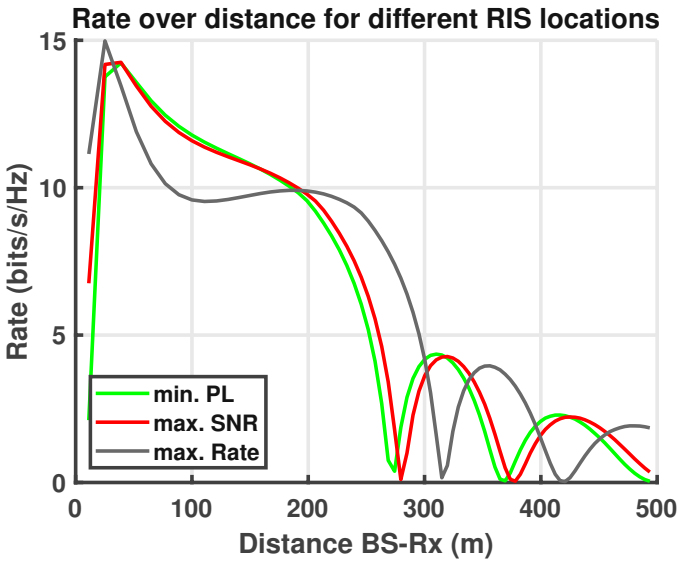

Figure 4.9: Rate over distance for the RMa LOS PL model and indirect beamforming.

Optimization criteria	Average-rate in bits/s/Hz
Minimum path loss	4.67
Maximum avg. received SNR	4.90
Maximum rate	5.29

Table 4.5: Average-rate comparison for the three RIS positions with the RMa PL model and LOS.

4.4.7 Further restrictions

There are some valid arguments that can further restrict the RIS placement. One powerful argument is, that not all tracks positions might be considered as relevant, because direct beamforming from the base station to the train could perform better close to the base station. This argument is indeed true and not only restricted to positions close to the base station as the upcoming section will show. To look into this argument a bit further is problematic as of right now, because to know where the RIS is placed optimally requires knowing in which locations the beamforming towards the RIS performs better, than beamforming directly to the train. This would result in an iterative problem, which can be avoided by combining the LOS and NLOS path loss models as in Section 4.7.
A second argument can be brought up by restricting the search close to the base station and LOS line as it is more likely that the optimal RIS position might be around these areas.

4.5 Direct and indirect beamforming

The goal of using a RIS in the railroad scenario is to improve the system performance in terms of BER and receive SNR. In order to reach this goal, it is crucial to determine if beamforming towards the RIS or towards the train is better. The former case is considered as indirect beamforming, whereas the latter is called direct beamforming. The performance of indirect beamforming is heavily dependent on the RIS position hence this was extensively discussed in the previous section. Both schemes rely on a different precoding vector for beamforming $\boldsymbol{f} \in \mathbb{C}^{N_{Tx} \times 1}$, where N_{Tx} is the number of transmit antennas. The precoding vector for the indirect transmission is given by

$$\boldsymbol{f} = \frac{1}{\sqrt{N_{Tx}}} \boldsymbol{a_{BS}}(\theta_{Tx}), \tag{54}$$

with the angle of departure from the base station to the RIS θ_{Tx} and the array response vector given in Equation (3). In the case of direct beamforming the precoding vector is given by

$$\boldsymbol{f} = \frac{1}{\sqrt{N_{Tx}}} \boldsymbol{a_{BS}}(\theta_{DIR}) \tag{55}$$

with the angle of departure from the base station to the train θ_{DIR}.
The goal of this section is to see in which region it is worth using indirect beamforming considering the RIS placement from the previous section and the available path loss models, i.e. RMa or UMa with LOS/NLOS. For now, each path loss model is considered as a separate scenario in order to be as standard compliant as possible, which leads to the following configurations for rural area simulations:

- RMa LOS with direct beamforming
- RMa LOS with indirect beamforming
- RMa NLOS with direct beamforming
- RMa NLOS with indirect beamforming

Note that over the entire railway positions either LOS or NLOS is assumed for all links. That means, in these simulations it is not possible that one link is in LOS and another link in NLOS. In Table 4.6 is an overview of the parameters used for the simulations.

Carrier frequency	$2.5\,\text{GHz}$
K_{sd} LOS	$30\,\text{dB}$
K_{sr} LOS	$30\,\text{dB}$
K_{rd} LOS	$30\,\text{dB}$
K_{sd} NLOS	$3\,\text{dB}$
K_{sr} NLOS	$3\,\text{dB}$
K_{rd} NLOS	$3\,\text{dB}$
θ_0	$\frac{\pi}{4}$

Transmit antennas	16
Receive antennas	1
Number of RIS elements	100
Transmit power	$20\,\text{dBm}$
Noise power	$-85\,\text{dBm}$
Antenna spacing (BS)	$\frac{\lambda}{2}$
Element spacing (RIS)	$\frac{\lambda}{2}$
RIS Position (rate)	$(120, 205)$

Table 4.6: Simulation parameters for direct and indirect beamforming with the RMa PL model.

Figure 4.10 shows the SNR over the distance between the base station and the train. In case of LOS the direct beamforming performs better than the indirect beamforming at every point. This suggests that the RIS might not improve the system performance at all. In case of NLOS simulations a similar trend holds true.
Figure 4.11 is the same plot as Figure 4.10, but with additional information about second order statistics. More specifically, the standard deviation at some points is included in form of error bars, where the length of a bar is two times the standard deviation. Note that the error bars are asymmetric due to the logarithm. In order to explain the asymmetric error bars consider the following example:
We assume a sample mean with $\bar{x} = 100$ and a standard deviation $\sigma = 10$. The standard deviation in case of a Gaussian distribution includes around 68% of all values, which means

$$[\bar{x} - \sigma, \bar{x} + \sigma] = [90, 110]\,, \tag{56}$$

are within this range. Taking the logarithm of these values result in

$$[\log_{10}(90)\,, \log_{10}(110)] = [1.95, 2.04]\,, \tag{57}$$

thus the error bars are asymmetric.

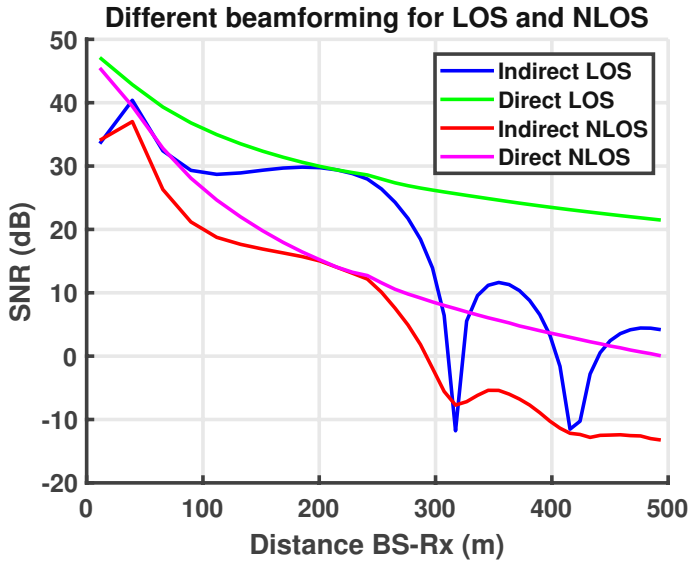

Figure 4.10: SNR over distance for direct and indirect beamforming with the RMa PL model.

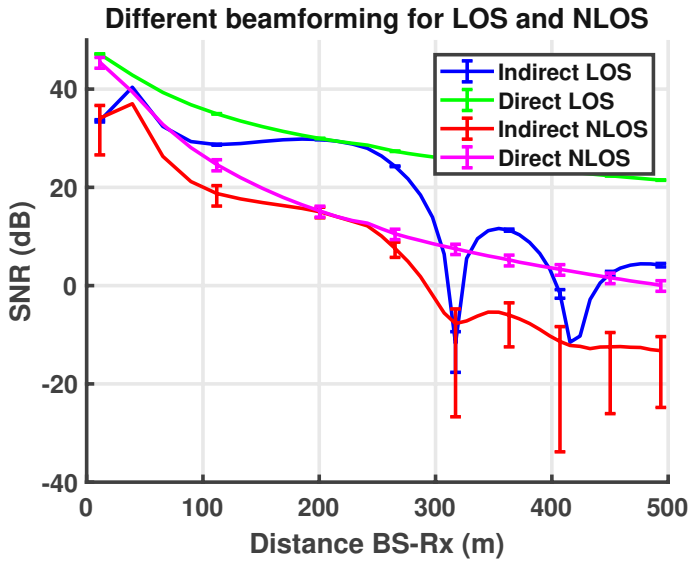

Figure 4.11: SNR over distance for direct and indirect beamforming with the RMa PL model including the standard deviation as error bars.

The question which arises now is why should you then place a RIS or what needs to be changed in order to actually get a performance gain? The first thing which comes into play is the number of RIS elements N, as the (beamforming) gain of the RIS depends on this parameter. A second argument is that the PL models in a realistic scenario should be modified such that the PL is increased as soon as the LOS between the base station and receiver is lost. These are the topics of the two upcoming sections.

4.6 Reasonable number of RIS elements

The number of RIS elements N has an impact on the (beamforming) gain from the RIS. As discussed in Section 3.3 a quadratic beamforming gain can be observed for optimal phase shifts. This means if the gain can be approximated as

$$G_{RIS}^{(dB)} \approx 10 \cdot \log_{10}\left(N^2\right), \tag{58}$$

increasing the number of elements N would always result in a better performance. However, there has to be a limit. In this section, this limit will be derived from the physical array size of the RIS. A quadratic structure is assumed alongside an element spacing of $\frac{\lambda}{2}$. As the wavelength λ depends on the carrier frequency f_c with $c_0 = \lambda \cdot f_c$, the side length can be described as

$$l_{RIS} = N \cdot \frac{\lambda}{2} = N \cdot \frac{c_0}{2 \cdot f_c}. \tag{59}$$

Limiting this side length to $6\,\text{m}$, seems like a reasonable physical limitation as this is already quite large compared with base stations. Considering the geometry of the scenario which consists of several hundred meters it is still small. For this limit on the side length the maximum amount of RIS elements for different carrier frequencies can be found in Table 4.7.

Frequency (GHz)	Maximum number of RIS elements N
0.8	32
2.5	100
5	200
28	1120
39	1560
60	2400

Table 4.7: Maximum number of RIS elements for different frequencies.

Even though a large surface area was considered, with a fixed element spacing there is a strict limitation in the possible gain from the RIS. This is especially troublesome for

high path loss in for example railroad scenarios, because a very high gain is needed. This problem of requiring large RIS arrays is also discussed in [34]. The author of the aforementioned paper was participating in designing and building a RIS in [17] for $5.8\,\text{GHz}$ with 1100 elements in a compact size of around $80\,\text{cm} \times 31\,\text{cm}$ by using varactor diodes. This was possible due to a smaller element spacing than $\frac{\lambda}{2}$. The measured power gain for this intelligent surface in the outdoor test was $14\,\text{dB}$, which is significantly lower than the approximated gain of $60.9\,\text{dB}$ from Equation (58). The reduction in power gain is definitely influenced by the reduced element spacing, which will be discussed in the next section.

4.6.1 Relevance of the element spacing for a RIS

Reducing the element spacing in order to obtain more RIS elements with a reasonable surface size is an approach in different literature sources such as [17] and [19]. With such a setup the beamforming gain of the surface will be reduced. To my knowledge there is currently no source available, which analyzes the impact of the element spacing for a RIS with respect to the power gain. For this reason and the similarity to a ULA an investigation based on a ULA seems reasonable. Authors of [35] and [36] figured out, that increasing the element spacing above $\frac{\lambda}{2}$ will sharpen the beam, which results in a higher directivity. The opposite happens while reducing the element spacing below $\frac{\lambda}{2}$. According to [35] a directivity loss of around $5.77\,\text{dB}$ is expected for an array of 64 elements while reducing the element spacing from $\frac{\lambda}{2}$ to $\frac{\lambda}{4}$. Until further investigation I suggest sticking with an element spacing of $\frac{\lambda}{2}$.

4.7 Combined path loss models

It is difficult to find measurement campaigns for path loss models in railway scenarios and a disappearing LOS channel in literature, because most papers build around viaduct and tunnel scenarios as in [37] or [38]. To account for the disappearing LOS in the scenario, an abrupt switch from the LOS to the NLOS is carried out. To make the scenario more clear, I want to emphasise that the indirect link always assumes LOS, i.e. from transmitter to RIS and then to receiver. The direct link, i.e. from transmitter to receiver, assumes LOS until $210\,\text{m}$. After $210\,\text{m}$ NLOS in the direct link is assumed. This path loss model swap can be formulated as

$$PL_{sd} = \begin{cases} PL_{LOS} & 10\,\text{m} \leq d_{TxRx} \leq 210\,\text{m} \\ PL_{NLOS} & 210\,\text{m} \leq d_{TxRx} \leq 500\,\text{m} \end{cases}, \tag{60}$$

where PL_{LOS} and PL_{NLOS} are chosen from the according model, i.e. RMa or UMa, from Table 4.2 and d_{TxRx} is the distance between transmitter and receiver. The abrupt switch of Equation (60) is depicted in the blue curve in Figure 4.12 for the RMa PL

model and in Figure 4.13 for the UMa PL model. At a distance of around $210\,\mathrm{m}$ there is now a step of $13.6\,\mathrm{dB}$ for the RMa and $24.9\,\mathrm{dB}$ for the UMa model. From Figure 4.4 it is already known, that the difference between LOS and NLOS in case of UMa is larger compared to RMa. For both simulations the RIS is placed based on the rate criterion.

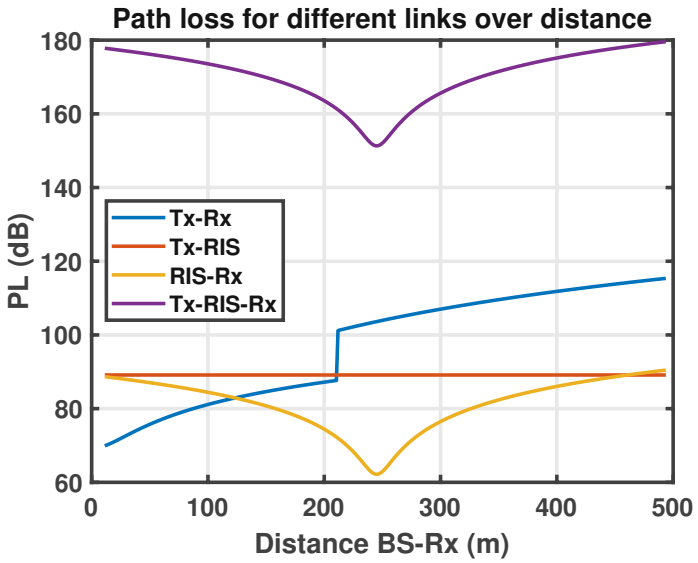

Figure 4.12: Path loss over distance for the RMa path loss model with a switch from LOS to NLOS.

This switch from the LOS to the NLOS model not only has an impact on the direct beamforming it also impacts the indirect beamforming as the channel is modeled with a direct component through $\boldsymbol{g_{sd}}$ in Equation (5).

4.8 Simulations for combined path loss models

Until now two different path loss models, namely RMa and UMa, have been introduced which include a switch from LOS to NLOS, in the direct link, after a certain distance. This was done to consider a use case of the RIS to overcome NLOS in a railroad scenario while using standard compliant path loss models. A heuristic RIS placement for three different criteria has been discussed and the importance of direct/indirect beamforming was pointed out. Still, a critical question remains: Is a performance gain with the RIS possible in a railroad scenario and how can it be achieved?
At first, I would like to show a simulation in terms of SNR over distance based on already known results. Strictly speaking the heuristic RIS position based on the rate criterion from Section 4.4.6 is used, combined with the path loss model from Section 4.7. This simulation for the rural macro path loss model can seen in Figure 4.14 with

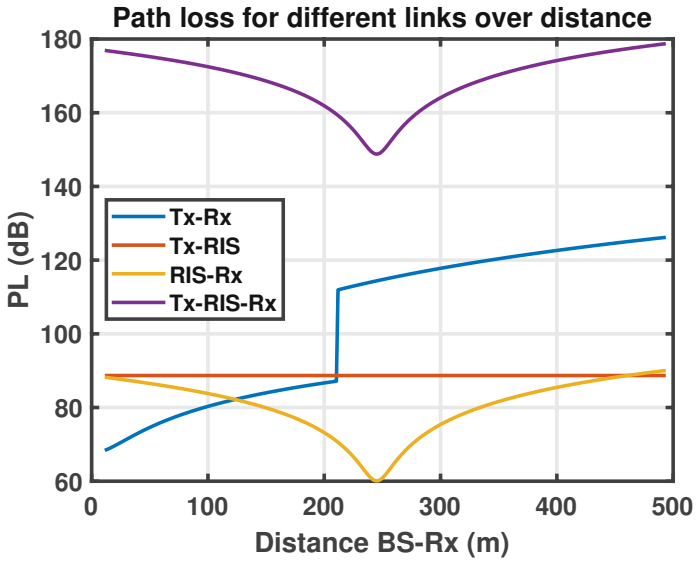

Figure 4.13: Path loss over distance for the UMa path loss model with a switch from LOS to NLOS.

the simulation parameters in Table 4.8. Note that two different K-factors on the direct link for NLOS are considered with $K_{sd} = 3\,\text{dB}$ in Figure 4.14(a) and $K_{sd} = -10\,\text{dB}$ in Figure 4.14(b). This is done to account for different types of blockages. The K-factor on the direct link until $210\,\text{m}$ is set to $K_{sd} = 30\,\text{dB}$, because LOS has not disappeared yet. The red curve in Figure 4.14 represents direct beamforming, while the blue curve shows indirect beamforming. At a distance of around $210\,\text{m}$ between the base station and train the LOS is lost and the path loss model swap happens for the direct link. Until this point, the direct beamforming clearly performs better than indirect beamforming. Around this point the performance of both schemes becomes similar as beamforming towards the RIS and towards the train is basically the same direction. After swapping to NLOS for the direct link, the SNR drastically decreases. The K-factor on the direct link K_{sd} has a major impact, because the SNR for $K_{sd} = -10\,\text{dB}$ after $210\,\text{m}$ is marginally different for direct and indirect beamforming. In contrary, the SNR has a difference of around $10\,\text{dB}$ for $K_{sd} = 3\,\text{dB}$ after the LOS has disappeared. Note the difference between Figure 4.14 and Figure 4.11 after $210\,\text{m}$. In Figure 4.11 indirect beamforming for LOS performed better at some points than direct beamforming for NLOS, which is not true in Figure 4.14 anymore. This is due to the fact, that the K-factor of the direct component K_{sd} is different, i.e. in Figure 4.11 $K_{sd} = 30\,\text{dB}$ for indirect beamforming and LOS whereas in Figure 4.14(a) $K_{sd} = 3\,\text{dB}$ for indirect beamforming after $210\,\text{m}$.

At this point it seems meaningless to deploy a RIS in a rural area. The next step is to

Carrier frequency	2.5 GHz
K_{sd} LOS	30 dB
K_{sr} LOS	30 dB
K_{rd} LOS	30 dB
K_{sd} NLOS	3 dB or -10 dB
K_{sr} NLOS	3 dB or -10 dB
K_{rd} NLOS	3 dB or -10 dB
θ_0	$\frac{\pi}{4}$

Transmit antennas	16
Receive antennas	1
Number of RIS elements	100
Transmit power	20 dBm
Noise power	-85 dBm
Antenna spacing (BS)	$\frac{\lambda}{2}$
Element spacing (RIS)	$\frac{\lambda}{2}$
RIS Position (rate)	$(120, 205)$

Table 4.8: Simulation parameters for the RMa and UMa PL model including the LOS to NLOS switch and RIS placement based on the rate criterion.

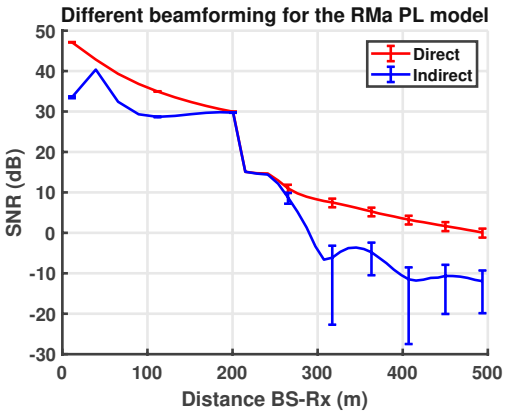

4.14(a): NLOS $K_{sd} = 3$ dB.

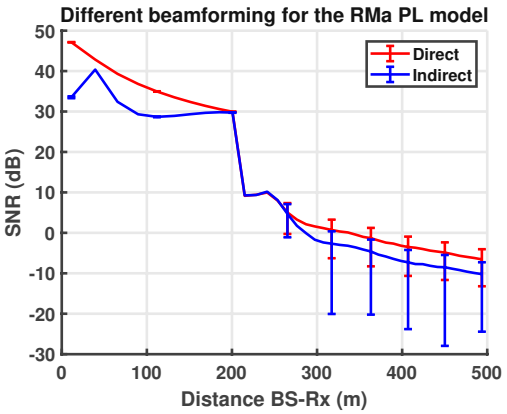

4.14(b): NLOS $K_{sd} = -10$ dB.

Figure 4.14: SNR over distance for the RMa PL model including the LOS to NLOS switch and the standard deviation as error bars.

analyze this behavior in the urban area, as the gap between the LOS and NLOS PL is larger and might bring the indirect beamforming closer to the direct beamforming. The same simulation parameter as in Table 4.8 are used. This simulation can be seen in Figure 4.15 and has basically the same problem as the simulation in case of the RMa PL model. Even tough the SNR at a distance of around $350\,\text{m}$ in Figure 4.15(b) is very low, the indirect beamforming performs very similar to the direct beamforming.

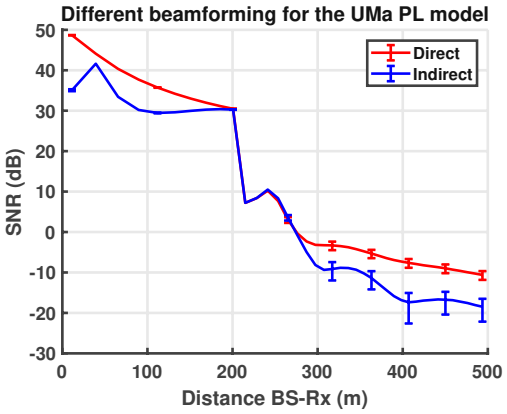

4.15(a): NLOS $K_{sd} = 3\,\text{dB}$.

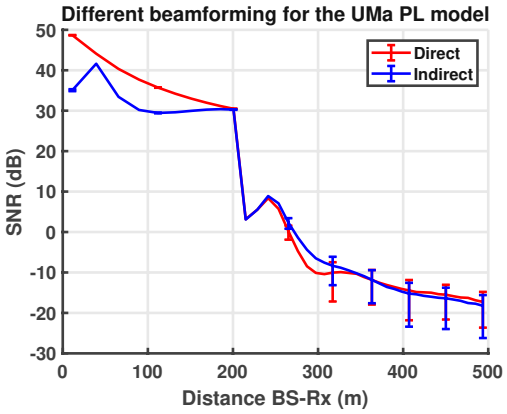

4.15(b): NLOS $K_{sd} = -10\,\text{dB}$.

Figure 4.15: SNR over distance for the UMa PL model including the LOS to NLOS switch and the standard deviation as error bars.

The underlying problem in these simulations is the high path loss. The path loss starts at a high value of around $56\,\text{dB}$ even for a small distance of $10\,\text{m}$. This makes it difficult for the indirect beamforming to perform better than direct beamforming for 100 RIS elements.

Consequences for beamforming

From Figure 4.14 and Figure 4.15 it is clearly visible that the direct beamforming in case of a railroad scenario and closer distances, i.e. below $210\,\text{m}$, performs better than indirect beamforming regardless of the path loss model. Considering the optimal RIS placement from Section 4.4 it will be more accurate to not consider all track positions in the optimization as in Equation (45). A better solution is to only consider the NLOS positions for the RIS placement. The set of all possible train positions excluding these where direct beamforming performs better, i.e. LOS from the base station to the train is available, can be formulated as

$$\mathcal{R}_{Train} = \left\{ \boldsymbol{r_{Train}} \in \mathbb{R}^2 \,|\, y_{Train} = 275 - 275 \exp\left(-\tfrac{1}{100} x_{Train}\right) \text{ and } x_{Train} > 100 \right\}. \quad (61)$$

With this in mind, it is most certainly better to use direct beamforming as long as LOS for the direct link is available. After the transition, it might be worth to use indirect beamforming.

4.8.1 Possible solutions to the path loss problem

Changing the path loss model from RMa to UMa has not resulted in a drastic change in performance. The huge path loss in the indirect link is the underlying problem. Generally speaking, there are several options that change this behavior, but not all of them are applicable to railroad scenarios. The three most important ones are discussed below and are based on the distance/frequency dependence of the path loss. There exist some other parameters in the path loss functions as seen in Table 4.2, which will be left out, because they have a minor impact on the magnitude.

Scaling distances

The first option would be to scale distances, as the path loss is amongst other things a function of the distance. Scaling the distances in a minor fashion might still result in a railroad scenario. Due to the considered geometry, the tracks should have a curved shape, such that the LOS disappears after a certain distance. If the scenario would be scaled down, than the train velocity has to be reduced, because a steeper turnaround would result in a higher centrifugal force. If the distances are scaled too much, then the scenario could be interpreted as a Vehicular-To-Infrastructure (V2I) or Car-To-Infrastructure (C2I) setup, which is not the topic of this thesis. As a result, scaling the distances is not applicable here.

Validating and potentially changing the NLOS PL model

To my knowledge there are no available measurement campaigns for a disappearing LOS in a railroad scenario with respect to path loss and/or K-factor. For this reason, I can not guarantee, that the used path loss model, especially in the NLOS case fits for a realistic railroad scenario. Unless the used model will be validated in the considered scenario, there might be other, probably more fitting, models such as the Stanford University Interim (SUI) model. This model has different terrain classifications. Type A is associated with hilly terrain and heavy foliage density. Measurements as in [39] showed, that such a model can be accurate for rural environments. With a different path loss model, the indirect beamforming could theoretically perform better, than the direct beamforming thus make the RIS viable in terms of performance.

Changing frequency

Another option is to lower the carrier frequency, because this would also lower the path loss. This option will be discussed extensively in the upcoming section.

Increasing the number of RIS elements

The last option is to increase the number of RIS elements N thus increase the beamforming gain of the RIS. This will also be discussed in the upcoming sections.

4.9 Simulations for reduced carrier frequency

The first candidate to solve the path loss problem is to reduce the carrier frequency. This would be a common solution in a rural environment, where the coverage area is large. The simulation setup has not changed, besides the carrier frequency and the RIS position. The carrier frequency has been reduced to $800\,\text{MHz}$ and the RIS position is determined by the rate criterion where only the NLOS train positions are considered. This was formulated mathematically by Equation (47) and Equation (61). Scaling the frequency down to $800\,\text{MHz}$ is only an exemplary solution as there are other possible frequencies. A list of frequencies for 4G and 5G systems can be found in [40] and [41], respectively.
A summary of the simulation parameters can be found in Table 4.9. Figure 4.16 depicts the difference between direct and indirect beamforming for $K_{sd} = 3\,\text{dB}$ and $K_{sd} = -10\,\text{dB}$. Especially in Figure 4.16(b) the performance of indirect beamforming is very similar to direct beamforming after the LOS of the direct link has disappeared. This does not justify a RIS placement based on the system performance, nevertheless a RIS provides other benefits for example in terms of security as already discussed in Section 2.1.4.

Carrier frequency	$0.8\,\text{GHz}$
K_{sd} LOS	$30\,\text{dB}$
K_{sr} LOS	$30\,\text{dB}$
K_{rd} LOS	$30\,\text{dB}$
K_{sd} NLOS	$3\,\text{dB}$ or $-10\,\text{dB}$
K_{sr} NLOS	$3\,\text{dB}$ or $-10\,\text{dB}$
K_{rd} NLOS	$3\,\text{dB}$ or $-10\,\text{dB}$
θ_0	$\frac{\pi}{4}$

Transmit antennas	16
Receive antennas	1
Number of RIS elements	100
Transmit power	$20\,\text{dBm}$
Noise power	$-85\,\text{dBm}$
Antenna spacing (BS)	$\frac{\lambda}{2}$
Element spacing (RIS)	$\frac{\lambda}{2}$
RIS Position (rate)	$(106, 194)$

Table 4.9: Simulation parameters for the RMa PL model including the LOS to NLOS switch and RIS placement based on the rate criteria for a reduced carrier frequency.

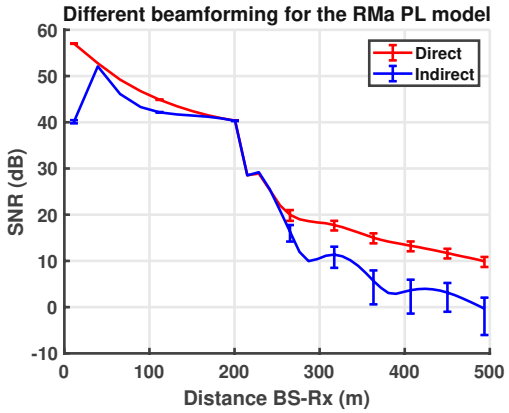

4.16(a): NLOS $K_{sd} = 3\,\text{dB}$.

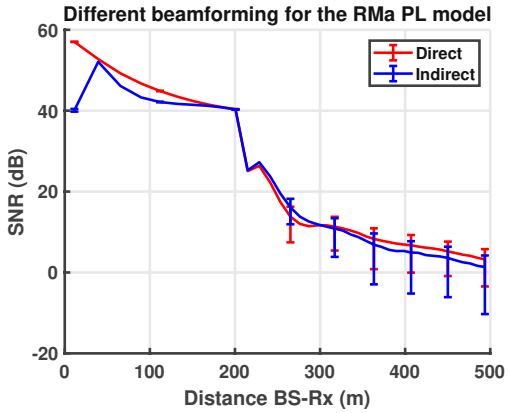

4.16(b): NLOS $K_{sd} = -10\,\text{dB}$.

Figure 4.16: SNR over distance for the RMa PL model for $800\,\text{MHz}$ and the standard deviation as error bars.

4.10 Simulations for increased number of elements

Decreasing the frequency did not result in the desired performance gain. The last option I want to discuss is to increase the number of elements. I chose the number of RIS elements for the carrier frequency of $2.5\,\text{GHz}$ based on a physical limited array size and a element spacing of $\frac{\lambda}{2}$, as discussed in Section 4.6. Additionally, in Section 4.6.1 the impact of the element spacing was discussed. However, most RIS-assisted wireless communication systems in literature assume a higher number of elements without considering the physical dimensions. Measurements for RISs with a high number of elements and a lower element spacing, such as in [17] have shown, that the beamforming gain of the RIS is reduced. As I do not want to exclude simulations with the common literature assumption in terms of RIS elements, I include simulations for 1024 and 2048 elements. This could be a solution in a dense urban environment, where higher carrier frequencies, thus smaller wavelength and RIS array size, are possible.
The simulation parameters are the same as in Table 4.8. The simulations for 1024 elements are depicted in Figure 4.17. These simulations show a performance gain on indirect beamforming after the LOS has disappeared. This gain becomes even more predominant for 2048 elements, which is shown in Figure 4.18.

4.11 Summary of most important findings

This chapter provided an overview of the performance of a RIS, if it has to serve an entire area to overcome NLOS situations. The surface is placed such that it always has LOS to the base station and to the train simultaneously. In contrary to the base station, which has a disappearing LOS after a certain distance of around $210\,\text{m}$. The scenario

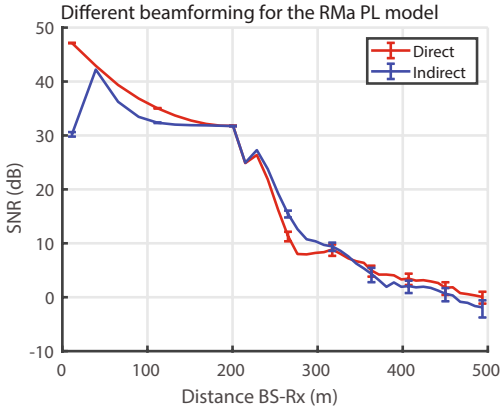

4.17(a): NLOS $K_{sd} = 3\,\text{dB}$.

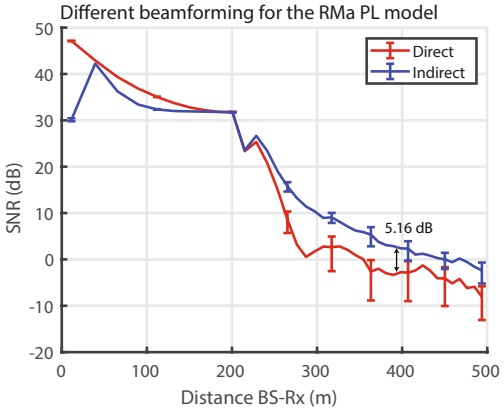

4.17(b): NLOS $K_{sd} = -10\,\text{dB}$.

Figure 4.17: SNR over distance for the RMa PL model for 1024 RIS elements and the standard deviation as error bars.

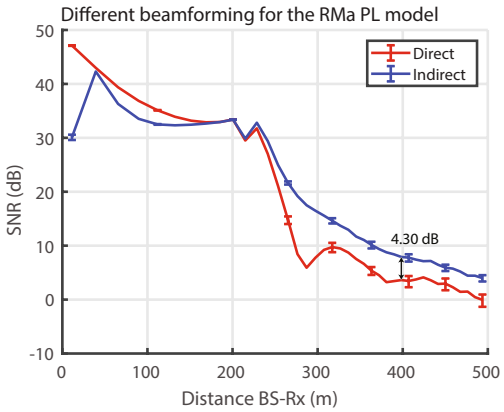

4.18(a): NLOS $K_{sd} = 3\,\text{dB}$.

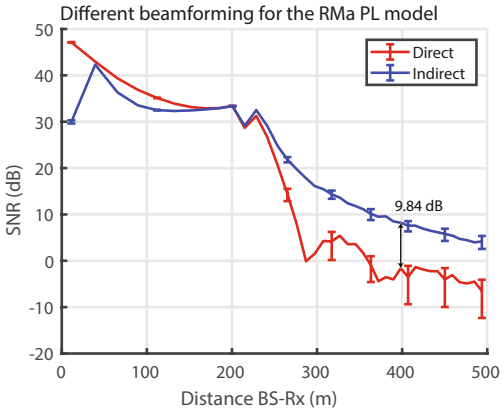

4.18(b): NLOS $K_{sd} = -10\,\text{dB}$.

Figure 4.18: SNR over distance for the RMa PL model for 2048 RIS elements and the standard deviation as error bars.

is inspired by a real-world situation, which was taken from OpenRailwayMap. After a necessary introduction of an underlying geometry and standard compliant path loss models from TR 38.901 V16.1.0, the importance of the RIS placement revealed itself. This topic was not considered in the previous chapter, because there was no underlying geometry needed. Three different placement strategies were discussed, namely the minimization of the overall path loss, the maximization of the average received SNR and the maximization of the rate. Simulations showed, that the rate maximization leads to the best performance in terms of average rate, thus this approach is kept until the end of this chapter. The rate is a common measure in literature to place wireless assisting devices such as RISs or relays.

A major problem in a RIS assisted wireless communication system are the path loss functions, because they start at a high magnitude of around $56\,\text{dB}$ even for the minimum required distance of $10\,\text{m}$. This amount of path loss for $2.5\,\text{GHz}$ is rough to overcome with the beamforming gain of the RIS, as this would require a high amount of elements and consequently a large RIS. In order to obtain a more realistic scenario, an abrupt switch from LOS to NLOS PL models for the direct link was introduced. After a first look at simulations, it became clear, that this setup will not be beneficial for a RIS. For the duration of an available LOS, the direct beamforming performed better at almost every location than the indirect beamforming. After the LOS disappeared, the performance in terms of SNR was drastically reduced, due to the high path loss.

A possible solution was discussed by reducing the carrier frequency and consequently the path loss. This change improved the performance of indirect beamforming for a low K-factor of $-10\,\text{dB}$ in the direct path. This improvement was not enough to increase the performance above direct beamforming, thus does not justify the placement of a RIS in order to improve the receive SNR.

Finally, another solution for increased number of RIS elements and a carrier frequency of $2.5\,\text{GHz}$ was discussed. In such a setup, the presence of the RIS has the potential of providing substantial gains compared to the case without it.

5 Conclusion

This thesis provided an overview of possible use cases for a RIS in a railroad environment. The approach to overcome NLOS situations was discussed in further detail. In this setup the RIS is placed in LOS to the base station and the user/train simultaneously. Contrary to the base station, which has a disappearing LOS to the user/train.
Starting with a link level analysis to get a basic understanding of the system model and different parameters. Under the assumption of a higher path loss of the NLOS direct link there was clearly a performance gain possible. Specifically, the square law from literature sources could be reproduced, i.e. every doubling of the number of RIS elements achieves about $6\,\mathrm{dB}$ power gain for optimized RIS phase shifts. The early research state of this technology comes with the problem of currently imperfect intelligent surfaces, which means that the common literature assumptions of non frequency-selective reflectivity and a continuous set of phase shifts might not be realistic. For this reason, the impact of these imperfections was discussed. A quantization of the phase states showed a minor degradation of the system performance. The reflectivity has several dependencies, such as frequency and phase shift, observed throughout literature. This thesis provided simulations for a reduced, but constant reflection coefficient.
The discussion was followed up with a system level analysis in a realistic railroad environment. The scenario was taken from OpenRailwayMap combined with 3GPP standard compliant path loss models and K-factors from railroad measurements. Three different placement strategies were discussed, because the RIS location has a major influence on the overall path loss of the indirect link. The position according to the common rate criterion performed best in terms of rate, thus this scheme was used until the end of the chapter. A major problem, even for a heuristically optimized RIS position, is the high path loss due to large distances. This limits the usefulness of a RIS in a railroad scenario with a moderate number of elements. A solution could be found by increasing the number of RIS elements to 2048 for a carrier frequency of $2.5\,\mathrm{GHz}$. This setup increased the received SNR drastically at the NLOS locations combined with indirect beamforming thus provided substantial gains compared to the case without a RIS.

5.1 Improvements

This section provides an overview of possible improvements in the existing scenario in order to make it more realistic.
On the one hand, it might make the scenario more realistic when a receive sided beamforming is introduced, such that a gain and additional degrees of freedom are created. On the other hand, both schemes, i.e. direct and indirect beamforming, should benefit from this in the same way thus the outcome of the simulations should not change.

A more costly, but surely worthy improvement would be the validation of the used path loss models. Throughout the last chapter it became clear, that the path loss is a major limiting factor. The used path loss models are standard compliant models for LOS and NLOS, respectively. Nevertheless they are not specifically for railroad with a disappearing LOS, thus a validation by measurement campaigns would either strengthen or weaken the findings in this thesis. If the path loss models fit the measurements well, then the only way of improving the system performance, while using a RIS to overcome NLOS situations, is connected with a high number of RIS elements. This argument also holds true when the path loss from the measurement is higher than the path loss from the model. Should the measurements show the contrary, then a reevaluation is recommended.
The system level simulations did consider movement in terms of static snapshot simulations. However, this is not the whole story, if one wants to consider movement. To get a better representation the channel model should account for microscopic fading due to Doppler-shifts of the signal. This opens up the possibility of researching the impact of a RIS for microscopic fading of the overall channel.
Last but not least I want to mention, that it is worth investigating the performance impact of a RIS in an environment which considers interferers. It is known from [42], that using a RIS with a low amount of elements might result in a performance degradation in terms of Signal-To-Interference-Plus-Noise Ratio (SINR) compared to not using a RIS while interference is present.

5.2 Outlook

Besides the aforementioned improvements to the existing scenario, there is an alternative setup that looks appealing. This setup is based on the concept of a STAR-RIS, which can be used as a lens. The company NTT DOCOMO proofed this, as already explained in Chapter 2. The downside is, that this company has not released technical details of their technology. A noteworthy use case is depicted in Figure 5.1 and Figure 5.2. This setup is different from the discussed scenario in this thesis, because it does not try to overcome NLOS situations. The STAR-RIS is placed above the tracks, such that it can be used as a reflector before the train passes by. After this event, the surface can be used as a lens to form a beam towards the train and effectively act as a range extender. The performance in the transition region is currently a bit unclear, as this requires near field investigations of a STAR-RIS.

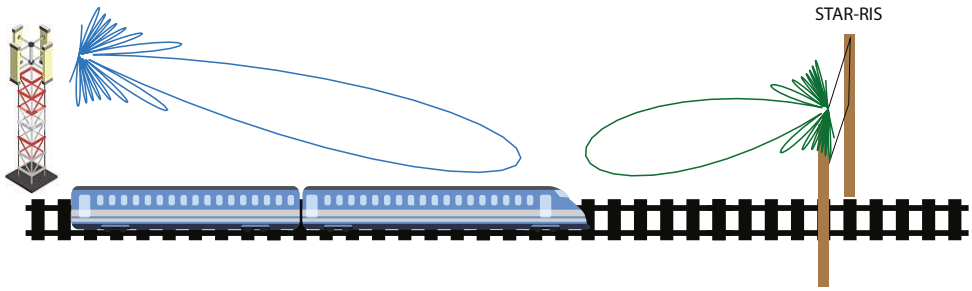

Figure 5.1: Reflective use case of a STAR-RIS before the train passes by the surface.

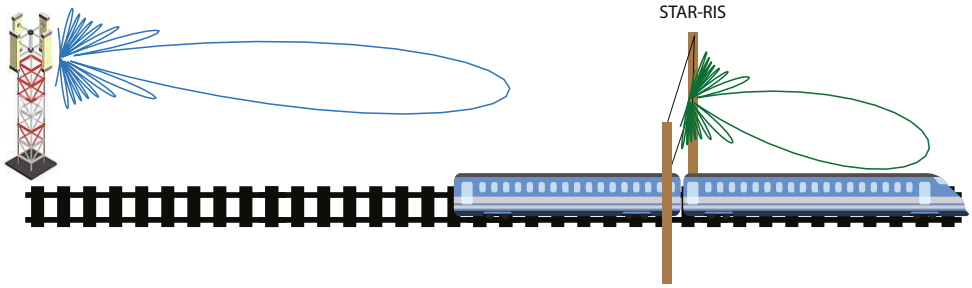

Figure 5.2: Transmissive use case of a STAR-RIS after the train passes by the surface.

6 References

[1] Y. Liu, X. Liu, X. Mu, T. Hou, J. Xu, Z. Qin, M. Renzo, and N. Al-Dhahir, "Reconfigurable intelligent surfaces: Principles and opportunities," *arXiv: Signal Processing*, 2020.

[2] Q. Wu, S. Zhang, B. Zheng, C. You, and R. Zhang, "Intelligent reflecting surface aided wireless communications: A tutorial," *CoRR*, vol. abs/2007.02759, 2020.

[3] E. Basar, M. Di Renzo, J. De Rosny, M. Debbah, M.-S. Alouini, and R. Zhang, "Wireless communications through reconfigurable intelligent surfaces," *IEEE Access*, vol. 7, pp. 116 753–116 773, 2019.

[4] MATLAB, *version 9.5.0.944444 (R2018b)*. Natick, Massachusetts: The MathWorks Inc., 2018.

[5] C. Huang, S. Hu, G. C. Alexandropoulos, A. Zappone, C. Yuen, R. Zhang, M. D. Renzo, and M. Debbah, "Holographic MIMO surfaces for 6G wireless networks: Opportunities, challenges, and trends," *IEEE Wireless Communications*, vol. 27, no. 5, pp. 118–125, 2020.

[6] Pivotal Commware. (2019) Holographic beam forming and phased arrays. https://pivotalcommware.com/wp-content/uploads/2019/10/HBF-vs-APA-White-Paper-2019.pdf.

[7] NTT DOCOMO. (2021, Jan.) DOCOMO and AGC use metasurface lens to enhance radio signal reception indoors. https://www.nttdocomo.co.jp/english/info/media_center/pr/2021/0126_00.html.

[8] X. Yu, D. Xu, and R. Schober, "Enabling secure wireless communications via intelligent reflecting surfaces," in *2019 IEEE Global Communications Conference (GLOBECOM)*, 2019, pp. 1–6.

[9] J. Qiao and M.-S. Alouini, "Secure transmission for intelligent reflecting surface-assisted mmwave and terahertz systems," *IEEE Wireless Communications Letters*, vol. 9, no. 10, pp. 1743–1747, 2020.

[10] Y. Liu, X. Mu, J. Xu, R. Schober, Y. Hao, H. V. Poor, and L. Hanzo, "STAR: simultaneous transmission and reflection for 360° coverage by intelligent surfaces," *CoRR*, vol. abs/2103.09104, 2021.

[11] J. Xu, Y. Liu, X. Mu, and O. Dobre, "STAR-RISs: Simultaneous transmitting and reflecting reconfigurable intelligent surfaces," *IEEE Communications Letters*, vol. PP, pp. 1–1, 01 2021.

[12] J. Kennington, E. Olinick, and D. Rajan, *Wireless Network Design: Optimization Models and Solution Procedures*. Springer Publishing Company, Incorporated, 01 2012.

[13] Z. Zhou, N. Ge, W. Liu, and Z. Wang, "RIS-aided offshore communications with adaptive beamforming and service time allocation," in *ICC 2020 - 2020 IEEE International Conference on Communications (ICC)*, 2020, pp. 1–6.

[14] M. Jung, W. Saad, M. Debbah, and C. S. Hong, "On the optimality of reconfigurable intelligent surfaces (RISs): Passive beamforming, modulation, and resource allocation," *CoRR*, vol. abs/1910.00968, 2019.

[15] J. Wu, Z. Shen, S. Ge, B. Chen, Z. Shen, T. Wang, C. Zhang, W. Hu, K. Fan, W. Padilla, Y. Lu, B. Jin, J. Chen, and P. Wu, "Liquid crystal programmable metasurface for terahertz beam steering," *Applied Physics Letters*, vol. 116, no. 13, p. 131104, 2020.

[16] X. He, "Tunable terahertz graphene metamaterials," *Carbon*, vol. 82, pp. 229–237, 2015.

[17] X. Pei, H. Yin, L. Tan, L. Cao, Z. Li, K. Wang, K. Zhang, and E. Björnson, "RIS-aided wireless communications: Prototyping, adaptive beamforming, and indoor/outdoor field trials," *arXiv: Computer Science*, 2021.

[18] W. Tang, X. Li, J. Y. Dai, S. Jin, Y. Zeng, Q. Cheng, and T. J. Cui, "Wireless communications with programmable metasurface: Transceiver design and experimental results," *China Communications*, vol. 16, no. 5, pp. 46–61, 2019.

[19] W. Tang, M. Z. Chen, X. Chen, J. Y. Dai, Y. Han, M. Di Renzo, Y. Zeng, S. Jin, Q. Cheng, and T. J. Cui, "Wireless communications with reconfigurable intelligent surface: Path loss modeling and experimental measurement," *IEEE Transactions on Wireless Communications*, vol. 20, no. 1, p. 421–439, Jan 2021.

[20] W. Tang, J. Y. Dai, M. Z. Chen, K.-K. Wong, X. Li, X. Zhao, S. Jin, Q. Cheng, and T. J. Cui, "MIMO transmission through reconfigurable intelligent surface: System design, analysis, and implementation," *IEEE Journal on Selected Areas in Communications*, vol. 38, no. 11, pp. 2683–2699, 2020.

[21] L. Dai, B. Wang, M. Wang, X. Yang, J. Tan, S. Bi, S. Xu, F. Yang, Z. Chen, M. D. Renzo, C.-B. Chae, and L. Hanzo, "Reconfigurable intelligent surface-based wireless communications: Antenna design, prototyping, and experimental results," *IEEE Access*, vol. 8, pp. 45 913–45 923, 2020.

[22] J. He, H. Wymeersch, T. Sanguanpuak, O. Silv'en, and M. Juntti, "Adaptive beamforming design for mmWave RIS-aided joint localization and communication," *2020 IEEE Wireless Communications and Networking Conference Workshops (WCNCW)*, pp. 1–6, 2020.

[23] OpenStreetMap. (2021, Jun.) OpenRailwayMap. https://www.openrailwaymap.org/.

[24] Q. Wu and R. Zhang, "Intelligent reflecting surface enhanced wireless network via joint active and passive beamforming," *IEEE Transactions on Wireless Communications*, vol. 18, no. 11, pp. 5394–5409, 2019.

[25] ——, "Towards smart and reconfigurable environment: Intelligent reflecting surface aided wireless network," *IEEE Communications Magazine*, vol. 58, no. 1, pp. 106–112, 2020.

[26] S. Abeywickrama, R. Zhang, Q. Wu, and C. Yuen, "Intelligent reflecting surface: Practical phase shift model and beamforming optimization," *IEEE Transactions on Communications*, vol. 68, no. 9, pp. 5849–5863, 2020.

[27] 3GPP, "Evolved Universal Terrestrial Radio Access (E-UTRA); Physical layer procedures," https://portal.3gpp.org/desktopmodules/Specifications/SpecificationDetails.aspx?specificationId=2427, 3rd Generation Partnership Project (3GPP), Technical Specification (TS) 36.213, 11 2020, version 16.3.0.

[28] ——, "Study on channel model for frequencies from 0.5 to 100 GHz," https://portal.3gpp.org/desktopmodules/Specifications/SpecificationDetails.aspx?specificationId=3173, 3rd Generation Partnership Project (3GPP), Technical Report (TR) 38.901, 01 2020, version 16.1.0.

[29] R. He, Z. Zhong, B. Ai, and J. Ding, "Distance-dependent model of Ricean k-factors in high-speed rail viaduct channel," in *2012 IEEE Vehicular Technology Conference (VTC Fall)*, 2012, pp. 1–5.

[30] S. Schwarz, E. Zöchmann, M. Müller, and K. Guan, "Dependability of directional millimeter wave vehicle-to-infrastructure communications," *IEEE Access*, vol. 8, pp. 53 162–53 171, 2020.

[31] E. Zöchmann, J. Blumenstein, R. Marsalek, M. Rupp, and K. Guan, "Parsimonious channel models for millimeter wave railway communications," in *2019 IEEE Wireless Communications and Networking Conference (WCNC)*, 2019, pp. 1–6.

[32] K. Ntontin, A.-A. A. Boulogeorgos, D. G. Selimis, F. I. Lazarakis, A. Alexiou, and S. Chatzinotas, "Reconfigurable intelligent surface optimal placement in

millimeter-wave networks," *IEEE Open Journal of the Communications Society*, vol. 2, pp. 704–718, 2021.

[33] Ö. Özdogan, E. Björnson, and E. Larsson, "Using intelligent reflecting surfaces for rank improvement in MIMO communications," *ICASSP 2020 - 2020 IEEE International Conference on Acoustics, Speech and Signal Processing (ICASSP)*, pp. 9160–9164, 2020.

[34] E. Björnson, O. Özdogan, and E. G. Larsson, "Reconfigurable intelligent surfaces: Three myths and two critical questions," *IEEE Communications Magazine*, vol. 58, no. 12, pp. 90–96, 2020.

[35] N. H. M. Adnan, I. M. Rafiqul, and A. H. M. Z. Alam, "Effects of inter element spacing on large antenna array characteristics," in *2017 IEEE 4th International Conference on Smart Instrumentation, Measurement and Application (ICSIMA)*, 2017, pp. 1–5.

[36] S. F. Maharimi, M. F. Jamlos, M. F. A. Malek, and S. C. Neoh, "Impact of number elements on array factor in linear arrays antenna," in *2012 IEEE 8th International Colloquium on Signal Processing and its Applications*, 2012, pp. 296–299.

[37] R. He, Z. Zhong, B. Ai, and J. Ding, "An empirical path loss model and fading analysis for high-speed railway viaduct scenarios," *IEEE Antennas and Wireless Propagation Letters*, vol. 10, pp. 808–812, 2011.

[38] R. He, Z. Zhong, and b. ai, "Path loss measurements and analysis for high-speed railway viaduct scene," *IWCMC 2010 - Proceedings of the 6th International Wireless Communications and Mobile Computing Conference*, pp. 266–270, 01 2010.

[39] Y. Zakaria, J. Hosek, and J. Misurec, "Path loss measurements for wireless communication in urban and rural environments," *American Journal of Engineering and Applied Sciences*, vol. 8, pp. 94–99, 04 2015.

[40] 3GPP, "Evolved Universal Terrestrial Radio Access (E-UTRA); User Equipment (UE) radio transmission and reception," https://portal.3gpp.org/desktopmodules/Specifications/SpecificationDetails.aspx?specificationId=2411, 3rd Generation Partnership Project (3GPP), Technical Specification (TS) 36.101, 04 2021, version 16.9.0.

[41] ——, "5G;NR; User Equipment (UE) radio transmission and reception;," https://portal.3gpp.org/desktopmodules/Specifications/SpecificationDetails.aspx?specificationId=3283, 3rd Generation Partnership Project (3GPP), Technical Specification (TS) 38.101-1, 04 2021, version 16.7.0.

[42] A. de Jesus Torres, L. Sanguinetti, and E. Björnson, "Electromagnetic interference in RIS-aided communications," *ArXiv*, vol. abs/2106.11107, 2021.

Table of Abbreviations

BBU Base Band Unit

BER Bit Error Rate

C2I Car-To-Infrastructure

CSI Channel State Information

CQI Channel Quality Indicator

DAS Distributed Antenna System

DL Downlink

HMIMOS Holographic Multiple Input Multiple Output Surface

IRS Intelligent Reflective Surface

LOS Line-Of-Sight

MCS Modulation and Coding Scheme

NLOS Non-Line-Of-Sight

PL Path Loss

RF Radio Frequency

RIS Reconfigurable Intelligent Surface

RRU Remote Radio Unit

RMa Rural Macro

SINR Signal-To-Interference-Plus-Noise Ratio

SNR Signal-To-Noise Ratio

STAR-RIS Simultaneous Transmitting and Reflecting Reconfigurable Intelligent Surface

SUI Stanford University Interim

TDD Time Division Duplex

ULA Uniform Linear Array

UMa Urban Macro

UL Uplink

V2I Vehicular-To-Infrastructure

VCCS Vienna Cellular Communications Simulators

3GPP 3rd Generation Partnership Project

5G 5th generation

6G 6th generation

List of Figures

List of Tables